TESIS DEFENDIDA POR

William Michael Thomas Zúñiga

Y APROBADA POR EL SIGUIENTE COMITÉ

Dr. Thomas Gunter Kretzschmar
Director del Comité

Dr. Stephen Vaughan Smith
Miembro del Comité

Dr. José Manuel Romo Jones
Miembro del Comité

Dra. María Tereza Cavazos Pérez
Miembro del Comité

MC. Francisco Suárez Vidal
Miembro del Comité

Dr. Thomas Gunter Kretzschmar
Coordinador del programa de posgrado en Ciencas de la Tierra

Dr. David Hilario Covarrubias Rosales
Director de Estudios de Posgrado

26 de febrero de 2010

CENTRO DE INVESTIGACIÓN CIENTÍFICA Y DE EDUCACIÓN SUPERIOR DE ENSENADA

PROGRAMA DE POSGRADO EN CIENCIAS EN CIENCIAS DE LA TIERRA

MOUNTAIN BLOCK RECHARGE IN THE SANTO TOMÁS VALLEY, BAJA CALIFORNIA, MÉXICO

TESIS

que para cubrir parcialmente los requisitos necesarios para obtener el grado de MAESTRO EN CIENCIAS

Presenta:

WILLIAM MICHAEL THOMAS ZUÑIGA

Ensenada, Baja California, México, febrero del 2010

ABSTRACT of the thesis presented by **William Michael Thomas Zúñiga** as a partial requirement to obtain the MASTER OF SCIENCE degree in EARTH SCIENCES with orientation in ENVIRONMENTAL GEOSCIENCES. Ensenada, Baja California, México, February 2010.

MOUNTAIN BLOCK RECHARGE IN THE SANTO TOMÁS VALLEY, BAJA CALIFORNIA, MÉXICO

Abstract Mountain block recharge (MBR) can be an important source of groundwater for alluvial aquifers in arid/semi-arid, mountainous regions. Unfortunately, geologic complexities within the mountain block often limit our understanding of this indirect form of recharge. Groundwater recharge in mountain-block dominated watersheds of northern Baja California relies on water contribution from the mountain system. Understanding the factors controlling MBR in these systems will help groundwater studies for this region. I have sampled and analyzed natural springs and wells throughout a mountainous sub watershed in the Santo Tomás Valley, Baja California, in order to understand the complex flow regimes that control MBR. Based on stable isotope, ion, and geologic data, three distinct water-types were found in the study area: 1) cold spring-type water, which represents local flow paths within the mountain block. These waters likely flow in faulted and fractured rock, and are considered focused and/or diffuse MBR; 2) thermal spring-type water, which represents regional flow. The source for these waters might originate from higher elevations (1100-1400+ meters above sea level). These altitudes are mostly found ~40 km east of the watershed boundary in the Sierra Juarez Mountain Range. The focused flow through the mountain-block is a deep water source that likely travels long distances through a complex fault/fracture system, and is considered focused MBR; 3) El Álamo-type water, which represents groundwater along the eastern edge of the watershed boundary, near the town of El Álamo. The water-type can be attributed to a diffuse recharge mechanism from high elevations (1300-1600+ meters above sea level) mostly found outside of the watershed boundary. Results for the El Álamo and thermal spring-type waters imply that the watershed boundary and the groundwater recharge boundary do not coincide for this area. The Santo Tomás Valley aquifer may receive a substantial amount of water from MBR. In addition, I show that one of the thermal spring's discharge (~3 l/s) is relatively steady year round, and successfully contributes groundwater (as focused MFR) to the local valley aquifer during "dry" years. The thermal spring-type water was also shown to be more significant than surfacing thermal springs; ambient temperature spring water and pond samples found near the thermal springs share the same, distant origin.

Keywords: Mountain-block recharge, mountain-front recharge, stable isotopes δD and $\delta^{18}O$, Santo Tomás Valley

RESUMEN de la tesis de **William Michael Thomas Zúñiga,** presentada como requisito parcial para la obtención del grado de MAESTRO EN CIENCIAS DE LA TIERRA con orientación en GEOCIENCIAS AMBIENTALES. Ensenada, Baja California, febrero de 2010.

Recarga del Bloque Montañoso en el Valle de Santo Tomás, Baja California, México

Resumen aprobado por:

_____

Dr. Thomas Kretzschmar
Director de Tesis

Resumen La recarga del bloque montañoso (RBM) puede ser una fuente importante de agua de subsuelo para los acuíferos aluviales en regiones montañosas áridas a semiáridas. Desafortunadamente, las complejidades geológicas dentro del bloque montañoso frecuentemente limitan la comprensión de esta forma de recarga indirecta. La recarga de agua de subsuelo en los terrenos montañosos de Baja California, depende del aporte de agua del bloque montañoso. En este trabajo se muestrearon y analizaron manantiales naturales y pozos dentro de una subcuenca hidrológica en el Valle de Santo Tomás, Baja California, con la finalidad de entender los complejos regímenes de flujo que controlan la RBM. Con base en isótopos estables, iones mayores y datos geológicos, se encontraron tres tipos distintos de agua en el área de estudio: 1) agua fría tipo manantial, que representa trayectorias de flujo local dentro del bloque montañoso. Estas aguas posiblemente fluyen a través de rocas falladas y fracturadas, y se les considera RBM focalizado o difuso; 2) agua termal tipo manantial, que representa flujo regional. La fuente de estas aguas probablemente se origina de elevaciones altas (1100-1400+ metros s.n.m.). Estas altitudes por lo general se encuentran a ~40 km al este del límite de la cuenca hidrológica en la coordillera montañosa de Sierra Juárez. Esta componente de bloque de montaña es una fuente de agua profunda que probablemente fluye grandes distancias a través de un sistema complejo de fallas y fracturas, y se le considera como una componente RBM focalizada; 3) el agua tipo El Álamo. Esta muestra de agua de subsuelo representa agua que fluye a lo largo del borde este de la cuenca hidrológica, cerca del pueblo de El Álamo. El agua probablemente experimenta recarga difusa de elevaciones altas (1300-1600+ metros s.n.m.) que la mayoría de las veces se encuentran fuera del límite de la cuenca hidrológica. Los resultados para las aguas tipo El Álamo y tipo manantiales termales indican que el límite de la cuenca hidrológica y el límite de la recarga de subsuelo no coinciden en esta área. El acuífero del Valle de Santo Tomás porconsiguiente recibe una cantidad mayor de agua de la RBM que, lo que previamente se pensaba. Además, se muestra que una de las descargas (~3 l/s) de manantiales termales es relativamente estable a lo largo del año, por lo que contribuye de manera importante con agua de subsuelo (como un RBM focalizado) al acuífero local del valle durante los años de sequía. Se observó también que el agua termal tipo manantial es más importante que los manantiales termales superficiales; los manantiales de agua a temperatura ambiente y las muestras de encharcamientos que se encontraron cerca de los manantiales termales comparten el mismo origen distante.
Palabras claves: Recarga bloque montañoso, isotopes estables δD and $\delta^{18}O$

Dedicatorias

Primeramente doy Gracias a Dios,
porque me ha bendecido grandemente, sin
su ayuda, jámas esto hubiera sido
posible.

Quiero dedicar este trabajo en memoria a mi abuelo José Zúñiga Lopez
que tanto cariño tuvo por estas tierras.

A mi tío Rigoberto Zúñiga Carballo
A mi primo Ulises Ojeda Zúñiga
A mi tío Eleazar Zúñiga Lagos
Por su aporte informativo y todo el apoyo
ncondicional que siempre me brindaron.

A mis padres, con mucho cariño
Michael y Minnie Thomas.

A Ana Laura, con todo mi amor, por
toda su ayuda y comprensión.

A mi hermana Kristen Michelle
y a su esposo Lionel Córdova
por sus valiosos consejos, que fueron
parte muy alentadora de mi progreso.

…

In memory of my grandparents William and Helen Thomas;
My uncle William Thomas;
And my uncle Kenneth Smith;

With love to my aunts Sue, Sally and Ellen;
And my Uncle Buzz;
My cousins Stacy, Ali, Jeff, Amy, Heather, Lauren, and their families.

…y Natasha.

Agradecimientos

Antes que nada quiero agradecer al Consejo Nacional de Ciencia y Tecnología (CONACYT), por el apoyo brindado durante estos dos años para la realización de este proyecto.

Al Centro de Investigación Científica y de Educación Superior de Ensenada (CICESE), por la facilidad del uso de las instalaciones computacionales y a su personal.

First, I would like to thank my advisor Dr. Thomas Kretzschmar and my committee members: Dr. José Romo Jones, M.C. Francisco Suárez Vidal, Dra. Ma. Tereza Cavazos and Dr. Stephen Smith. They have guided me through multiple thesis advances, and have helped me achieve this goal.

I would like to further express my appreciation to Dr. Stephen Smith. He helped revise my thesis multiple times throughout the study. Without him, I may not have learned some of the important skills in scientific writing and research.

I am grateful to M.C. Francisco Suarez for his help since my undergraduate thesis at SDSU.

I would like to specially thank Dr. Chris Eastoe for his hospitality and assistance throughout the thesis. His expertise helped guide me through a very interesting part of my study.

I'd like to thank Ramón Mendoza for sharing his knowledge in field geology, and assisting me throughout my thesis, and the daily realities of science and work.

My professors; I learned a great deal in and out of each of your classes: Dr. Enrique Trevino, Dr. John Fletcher, and Dr. Rogelio Vásquez. Thank you for your dedication.

Dr. Arturo Martín Barajas, for steering me in the right direction with my thesis.

I must thank everyone who helped me during my field work: Ulises Ojeda, Rigoberto Zúñiga, Don Luis, Felipe Vega, Mariana, and Addisu.

I want to also thank the staff who helped along the way: Jaime Calderon, Humberto Benitez, Alejandro Diaz, Mario Vega.

And, of course, to my fellow students and friends who have studied with me for the past 2 years. It's been fun.

Thanks

TABLE OF CONTENTS

TABLE OF CONTENTS (continued)

Page

LIST OF FIGURES

LIST OF FIGURES (continued)

LIST OF FIGURES (continued)

LIST OF FIGURES (continued)

LIST OF FIGURES (continued)

LIST OF TABLES

I. INTRODUCTION

I.1 Groundwater Recharge in Arid and Semi-Arid Regions

Increasing concern for groundwater management and sustainability in arid and semi-arid regions has recently led to many studies of groundwater recharge (Scanlon et al., 2006; Phillips et al., 2004; Eastoe et al., 2004). Groundwater recharge, however, is considered one the most difficult processes of the hydrological cycle to measure (Phillips et al., 2004). Arid and semi-arid regions exacerbate these difficulties, because high potential evapotranspiration (PET) rates typically exceed precipitation on a monthly basis, resulting in negligible (or no) recharge. Net infiltration is limited to extreme storm events and/or specific basin locations where water is less affected by elevated temperatures (Flint et al., 2004; Wilson and Guan, 2004).

Valley aquifers in mountainous watersheds are partially recharged via the mountain block and/or mountain front zone (Smerdon et al., 2008; Huntley, 1979; Thyne, 1999). Referred to as "mountain-front recharge (MFR) and/or mountain-block recharge (MBR)" (a further explanation of their differences are in section I.4), these types of aquifer replenishment are often considered dominant sources for groundwater in arid and semi-arid environments (Maurer et al., 1999; Wilson and Guan, 2004). However, due to the heterogeneous nature of mountain systems, rain infiltration does not occur in all places; thus, recharge is limited to specific basin locations, making MFR and MBR difficult component to measure (Flint et al., 2004). These locations might include heavily fractured areas with thin soils or focused flow along ephemeral or perennial streams. The increased permeability of the fractures and streambeds may lead to rapid infiltration, and ultimately recharge that is little affected by evaporation. These recharge contributions depend on the topography, rock type and vegetation of the mountain block and mountain front zone (Flint et at., 2004; Wilson and Guan, 2004).

Many methods are used to determine MFR and MBR, including: water balance, precipitation-runoff regression, chloride mass balance, Darcy's law, environmental tracers, etc (Wilson and Guan, 2004). Each approach has its strengths, but no method is without flaw. The precipitation-runoff regression model calculates stream runoff and channel infiltration; however, it is based on the assumption that the mountain block is impermeable (Wilson and Guan, 2004). Environmental tracers such as oxygen and hydrogen isotopes are used to determine areas of recharge, given that variations of $\delta^{18}O$ and δD in rainwater are influenced by altitude, latitude, evaporation and paleoclimatic effects, among other factors (Clark and Fritz, 1997; Eastoe et al., 2008; Wilson and Guan, 2004; Palmer, 2007). The method has many uses including: tracing MFR to alluvial aquifers, identifying recharge from basin vs. mountain precipitation, identifying local and regional flow systems in the mountainous terrains, and determining recharge from winter vs. summer rainfall (Eastoe et al., 2008; Wilson and Guan, 2004). (A further explanation is discussed in section I.5).

The importance of groundwater whose source originates in a mountain system (i.e., MBR) has been a subject of debate. This form of groundwater contribution can be difficult to quantify, leading to opposing arguments concerning its significance. While some studies disregard groundwater contribution from the mountain block, others consider it to be the dominant source of replenishment (Wilson and Guan, 2005). Manning and Solomon [2004] suggest that many MBR studies may have largely overestimated recharge, and typically contain uncertainties between 50-100%. Such overestimates raise question to its significance as a groundwater contributor. These inconsistencies may be due to study areas with distinct mountain-block characteristics (e.g., the ratio between the area of the mountain-block and the area of the valley floor). A study in the Silver Island Mountains, Utah, shows that in the fall of 2006, a mountain-block-dominated (35% bedrock) catchment received twice as much recharge (from the mountain system) when compared to an alluvial fan-dominated (10% bedrock) catchment (Carling, 2007). Additionally, permeability values in crystalline rock can vary by several orders of magnitude depending on the degree of fracturing (Caine, 1996), which may add to the conflicting results.

Determining whether MFR and MBR contributes significant amounts of water to valley aquifers is essential for accurate groundwater management in arid/semi-arid, mountainous regions. More importantly, understanding the geologic factors controlling this type of recharge will help to comprehend the complex hydrologic process within a mountain system.

I.2 Purpose and Objectives

Valley aquifers in the arid/semi-arid, mountainous region of northern Baja California may heavily depend on groundwater contribution from the mountain block. However, the mountain-block hydrologic system is not commonly studied in this region.

The purpose of this study is to better understand MBR in a mountain-block-dominated watershed in northern Baja California by analyzing and interpreting stable isotope ($\delta^{18}O$, δD) and hydrochemistry data of water samples within a mountainous watershed near the town of Santo Tomás. Additionally, detailed maps of the study area (e.g. topography, lineament, vegetation cover) will be used in conjunction with hydrogeology and hydrochemistry results from natural springs, groundwater, and stream runoff to help comprehend this complex type of recharge.

Due to large uncertainties concerning the relevance of MBR, I have used a qualitative approach to determine whether this type of recharge may be a significant source of groundwater for the alluvial aquifer. Questions of interest regarding MBR in the study area include:

1. What are the physical components controlling MBR in the study area (e.g., lithology, faulting etc.)?

2. What is the source of recharge (elevation, age, etc.) of the natural springs and groundwater in the basin?

3. What is the relationship between faults/fractures, vegetation and springs throughout the watershed?

4. Does spring water recharge the valley aquifer as MFR during arid months?

I.3 Study Area: Santo Tomás Valley

Santo Tomás Valley

Located ~150 km south of the U.S./México border in Baja California, México (Figure 1), the Santo Tomás Valley is a lightly populated, yet agriculturally productive area. The town of Santo Tomás is situated along the transpeninsular highway 1, ~40 km southeast of the coastal city of Ensenada. At 300 m elevation, the town is located ~30 km east of the Pacific Ocean, and is delineated by the coordinates: 116º 01' 55.20", 116º 41' 20.40" West and 31º 38' 35.52", 31º 20' 57.84" North (CONAGUA, 2008).

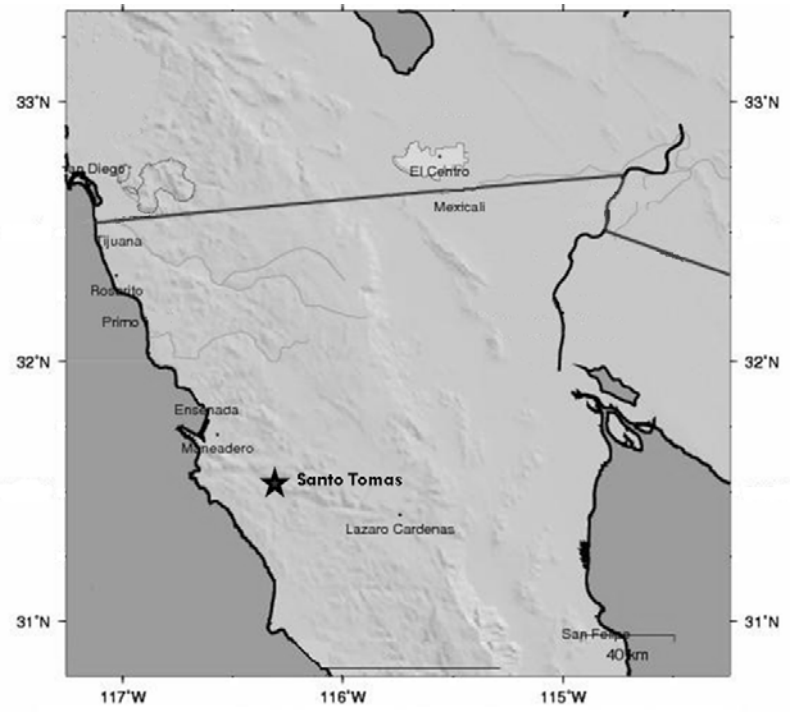

Figure 1. Location map of Santo Tomás, Baja California, Mexico. The town is located ~150 km south of the U.S./México border, and ~40 km southeast of the city of Ensenada.

Its relatively long, narrow valley floor covers ~40 km^2 of fertile soil, consisting of unconsolidated alluvium deposited by the Santo Tomás stream. For over 100 years the valley has been a large producer of wine, yet despite its importance to Baja California, the valley has not been heavily studied.

Santo Tomás Watershed

The Santo Tomás Valley's drainage basin covers ~700 km^2 (Figure 2), consisting mostly of volcaniclastic and plutonic rock surrounding the basin floor (Gastil, 1975). The drainage area (i.e. mountain-block) is about 17 times the valley area (denoted by the green polygon in Figure 2b). The bedrock-dominated watershed may highly favor MBR as a dominant contributor for groundwater.

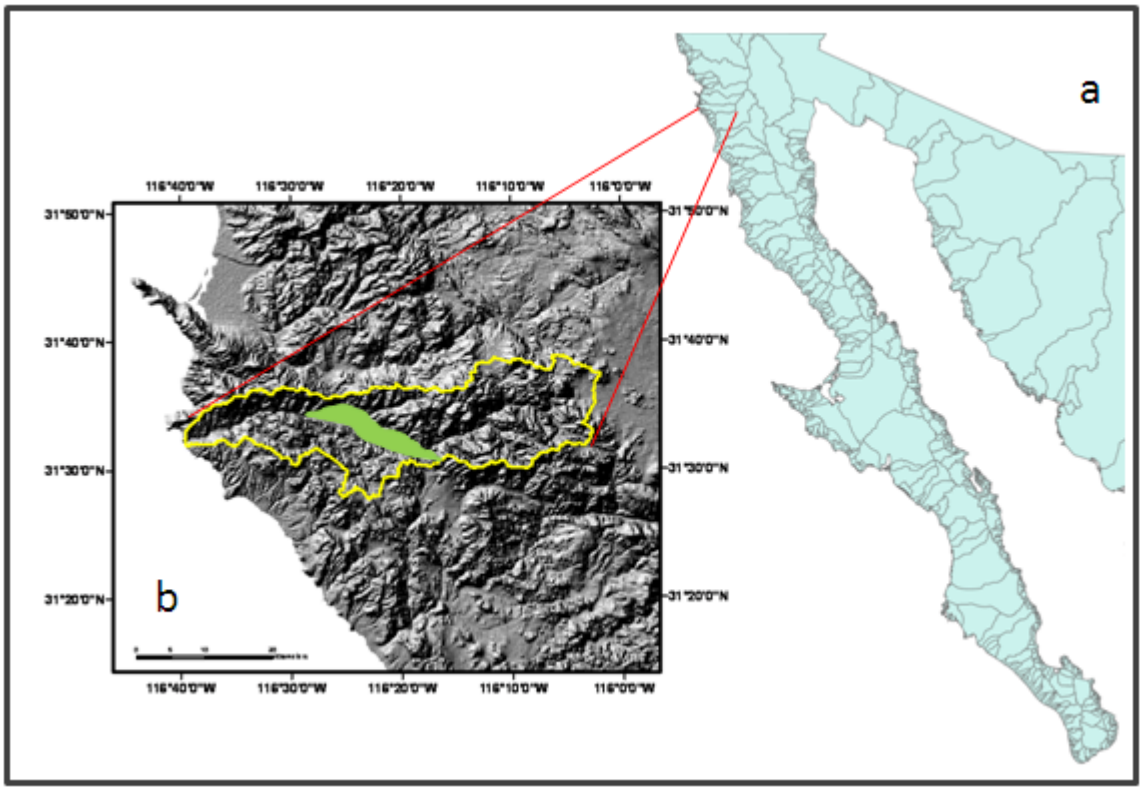

Figure 2. Santo Tomás watershed showing a) hydrologic watersheds of Baja California (1:25000) (CONAGUA); b) digital elevation model showing the Santo Tomás watershed boundary (~700 km^2).

The watershed consists of two distinct sections; a steep, mountainous eastern section where the headwaters of the Santo Tomás stream originate, and a gentler sloping western section, which includes the bulk of the valley floor (Figure 3).

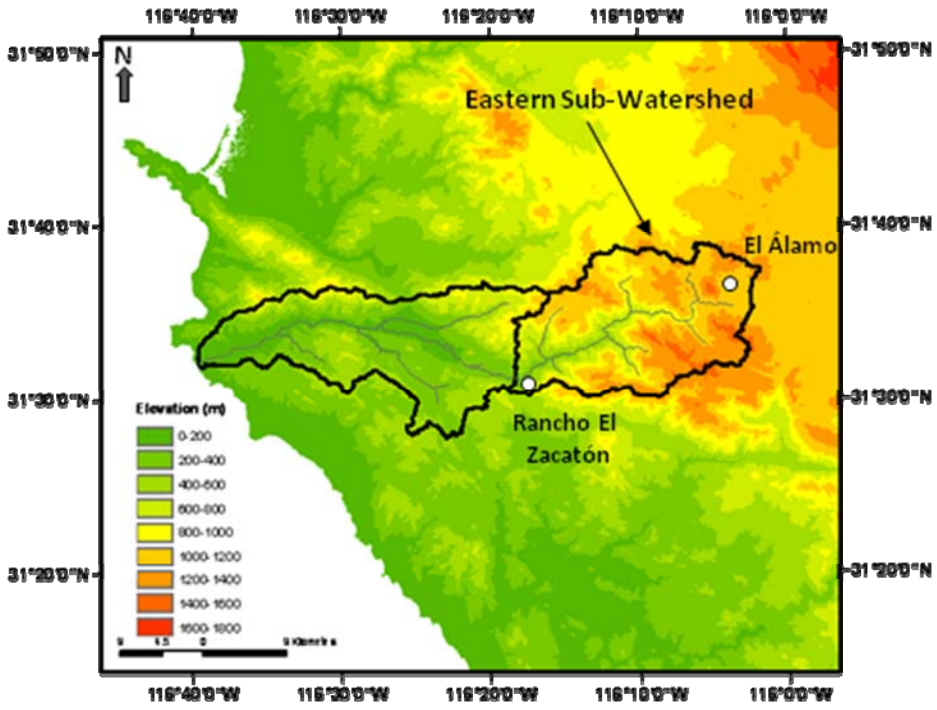

Figure 3. Elevation map created in ArcGis showing the Santo Tomás watershed and adjacent area. The watershed can be divided into eastern and western sub-watersheds. The area chosen for study is the eastern sub-watershed (~300 km^2) due to its mountainous terrain, which appears to favor MBR, considering the significant topographic relief. Geographically, the town of El Álamo and Rancho El Zacatón mark the eastern and western-most limits of the study area. Both end-points can be reached by vehicle, but rugged terrain between these two sites limits access to horseback or foot.

The focus of this work is in the eastern section of the Santo Tomás watershed (i.e. eastern sub-watershed), upstream from the bulk of the valley floor (Figure 3). Due to its extensive mountainous terrain, (~300 km), and minimal valley floor area, this section is favorable for studying the hydrologic processes within the mountain block (i.e. MBR). Note that the highest altitudes are found within the eastern sub-watershed (Figure 3).

The easternmost limit of the study area is in the abandoned gold mining town of El Álamo. This flat summit area (~10 km^2) quickly steepens as the Santo Tomás arroyo's

tributaries drop from the summit towards the west. The steep terrain terminates ~25 km downstream (to the west) where the arroyo changes directions slightly, and the bulk of the valley begins, near Rancho El Zacatón (Figure 3). This ranch marks the westernmost section of the study area.

Vehicle access is possible in and around El Álamo from the north, along highway 3; Rancho El Zacatón is accessible from the west, along highway 1. However, rugged terrain between these two sites limits access to foot or horseback.

Climate

Two weather stations, which provide meteorological data for the area, are located within the Santo Tomás watershed: The El Álamo station (~1100 m elevation), and Santo Tomás station (~300 m elevation).

Santo Tomás is characterized as arid to semi-arid, with highly variable annual precipitation, averaging ~200 mm/yr (CONAGUA, 2008) mostly from the fall-winter "wet" season. However, monsoon thunderstorms rising from the Gulf of California occasionally impact the eastern section of the Santo Tomás watershed. The Mediterranean climate of the valley averages 17.8°C, with August being the warmest month (24.5°C average) and January the coolest (12.3°C) (CONAGUA, 2008).

Geology

The fault-controlled Santo Tomás Valley is a pull-apart basin formed at a right step along the Agua Blanca fault (Gastil, 1975; Suárez, 1993) (Figure 4). Fed by the Santo Tomás stream, the basin aquifer consists of unconsolidated Quaternary alluvium, ranging in size from boulder (at its eastern edge) to clay (CONAGUA, 2008). The adjacent mountain block, east of the basin floor, consists mostly of crystalline rock associated with the Peninsular Ranges Batholith, (intrusive granitic and gabbroic rock). Pre-batholithic units include undifferentiated volcanic (Cretaceous Alisitos Formation) and metamorphic rock (Gastil, 1975). The Mesozoic Peninsular Mountain range, created by subduction of the ancient Farallon Plate, provides significant topographic relief within the watershed

(Figure 3) (Gastil, 1975). Extensive fracturing, associated with the Agua Blanca fault (discussed below), is widespread throughout the area, and might heavily influence groundwater flow

.

The Agua Blanca fault is located approximately 40 km south of Ensenada, Baja California. The fault strikes about N70°W, cutting across two-thirds of the northern section of the Baja peninsula. Its discontinuous 130 km length on land is partitioned into defined eastern, central and western zones; each approximately 35 km in length. The sections are characterized as right-stepping segments which give rise to valleys along the fault: San Matías, Trinidad, Agua Blanca and Santo Tomás (Allen et al., 1960; Suárez, 1993). The origin of this fault is believed to be associated with the subduction of the Farallon plate during the Mesozoic era (Gastil et al., 1975, Suárez et al., 1993), yet previous mapping of geomorphic features and trenching along the fault indicate the Holocene occurrence of major surface ruptures as well (Allen et al., 1960, Rockwell et al., 1993).

Hydrogeology

The Santo Tomás Valley aquifer covers ~40 km^2 of surface floor. This unconfined aquifer consists of gravel, sand, silt and clay sized particles. Samples taken by the National Water Commission (CONAGUA) from multiple wells within the valley range in pH from 7.2 – 8.3, electrical conductivity from 1.25 – 1.8 mS/cm (768-1150 ppm), and in temperature from 18.9 – 22.7°C (CONAGUA, 2008).

A total groundwater extraction of 1038.7 hm^3 was recorded for 2007 for the following uses: industrial (0.02%), service (0.02%), various (0.23%), domestic (0.45%), livestock (0.68%), urban (0.68%), and agriculture (98.29%) (CONAGUA, 2008). According to CONAGUA [2008] the aquifer has an annual deficit of 3.8 hm^3.

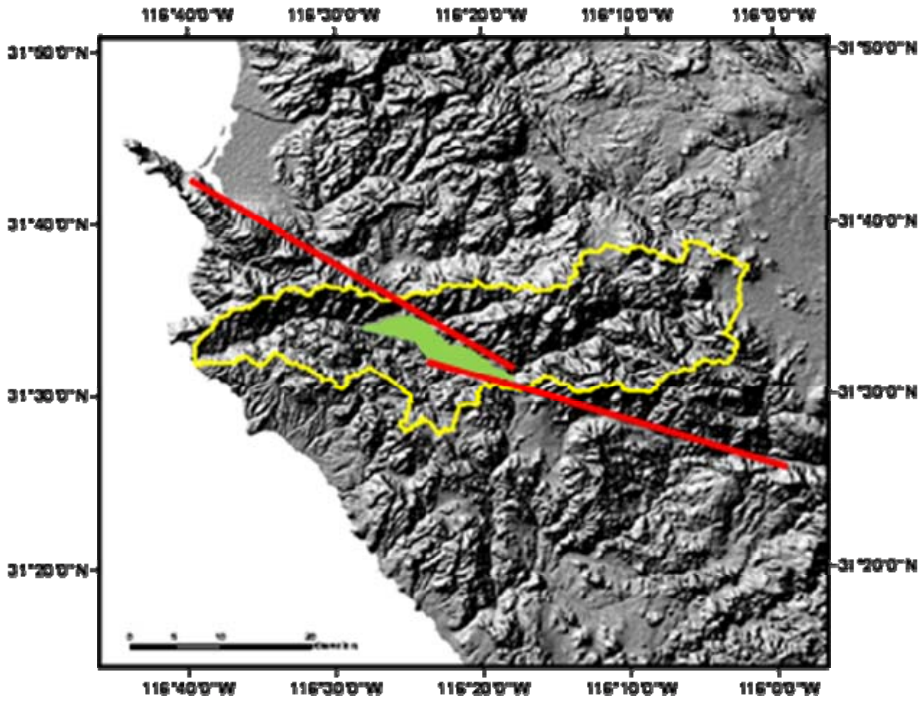

Figure 4. Digital elevation model showing the Santo Tomás watershed (yellow), the bulk of the valley floor (green) and two segments of the Agua Blanca fault (western and central). Note the right step between the central and western strands which gives rise to the "pull-apart" basin.

Figure 5. Santo Tomás Valley. Note the long narrow valley floor and steep adjacent mountain block.

I.4 Mountain-Front and Mountain-Block Recharge

Mountain front recharge is a general term introduced by Keith [1980] to describe groundwater recharge to valley aquifers in mountainous watersheds. The definitions used in this paper are consistent with those presented by Wilson and Guan (2004), who consider mountain front recharge as "all water with its source in the mountain front or mountain block".

Mountain front recharge can be divided into two categories: mountain-*front* recharge (MFR) and mountain *block*-recharge (MBR). From herein we will discuss mountain-front and mountain-block recharge as separate components.

The mountain-front component accounts for infiltration through ephemeral or perennial streams near the mountain front (Figure 6). This *near-surface* component is dominantly controlled by overland flow, and is often referred to as transmission losses (Wilson and Guan, 2004). Recharge, therefore, depends primarily on runoff and on the permeability of the streambed. Precipitation falling directly on the valley floor, or the mountain front zone, and infiltrating in place is also considered MFR (Figure 6) (Wilson and Guan, 2004).

MBR is a *sub-surface* process in which the valley aquifer is recharged from lateral inflow from the adjacent mountains (Figure 6, 7). This term does not include runoff; instead, it accounts for precipitation directly entering the mountain block, and depends primarily on the permeability of the mountain system (Wilson and Guan, 2004).

Both MFR and MBR have a *focused* and a *diffuse* component. Infiltration from overland flow in stream channels is considered a focused component of MFR (Wilson and Guan, 2004), and has been shown to be a substantial component of groundwater in arid and semi-arid environments (Wilson and Guan, 2004; Ponce et al., 1999). Moreover, even when ephemeral streams are dry, there is often a significant amount of interflow beneath the streambed recharging the valley aquifer (Wilson and Guan, 2004).

Precipitation falling directly on the valley floor or mountain front zone and recharging in-place is considered a diffuse component of MFR. This type of recharge is relatively minor in mountainous watersheds with small valley floors. The diffuse component also considers interflow in small unmapped channels near the mountain front (Wilson and Guan, 2004).

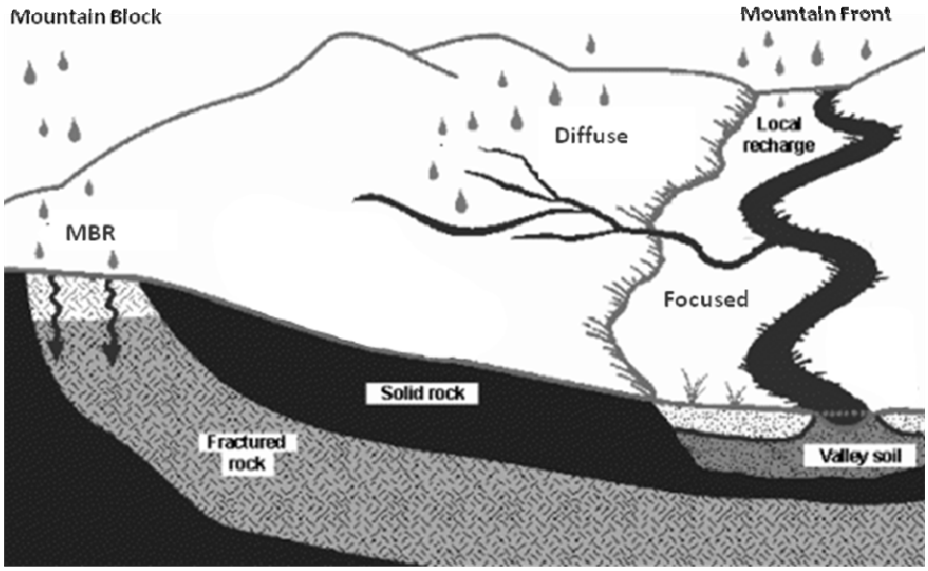

Figure 6. Schematic diagram of groundwater recharge via the mountain-front and mountain-block. Both focused mountain-front recharge and diffuse mountain-front recharge are shown. Only focused mountain-block recharge is shown (Image modified from Lyle Ramond Jr., 1988).

MBR considers the groundwater flow regime above the mountain front. The focused and diffuse components depend on the geologic factors controlling infiltration within the mountain block (Wilson and Guan, 2004). The diffuse component is characterized by water from the mountain block being transmitted into the adjacent valley aquifer through the bedrock. This process depends on the permeability of the lithologies that make up the mountain system (Wilson and Guan, 2004). For example, a semi-permeable volcanic tuff may have a considerable diffuse mountain-block component, whereas an un-weathered granitic block will display a negligible diffuse component. Ubiquitous fracturing commonly associated with rock types (e.g., basalts), will also favor diffuse MBR.

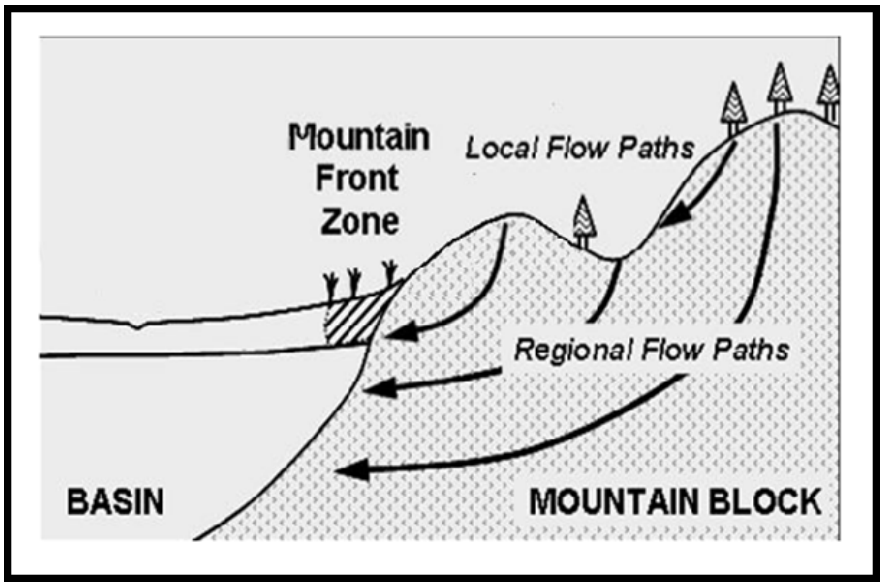

Figure 7. Schematic diagram of the diffuse mountain-block recharge component. The local flow paths exit as springs, whereas the regional flow paths recharge the valley aquifer with a lateral influx of water. (Modified from Toth [1963] and Keith [1980].

The focused component also depends on the permeability of the mountain block. However, this term accounts for infiltration of water via faults and fractures within the mountain system, which is considered secondary permeability. This component does not necessarily depend on the rock type, but rather on the degree of fracturing. This type of recharge becomes extremely difficult to measure due to the wide range of permeability in faults and fractured rock (Wilson and Guan, 2004; Caine, 1996).

Breaking down the terms into MFR and MBR can simplify the complexity of recharge in a mountainous watershed. Dividing recharge into the focused and diffuse groups also helps identify which geologic features are responsible for recharge. However, despite the distinctions between MFR and MBR, it is important to keep in mind that they often complement each another. For example, precipitation may infiltrate the mountain block through a fracture (a focused mountain- block component); however, instead of reaching the valley aquifer as sub-surface inflow, the water may surface as a spring. This spring water may eventually infiltrate into the valley via an ephemeral or perennial stream, which would be considered a focused mountain-front component.

I.5 Stable Isotopes: $\delta^{18}O$ and Deuterium (δD)

In 1961 Harmon Craig discovered that oxygen and hydrogen isotopes in fresh water fractionate in a predictable manner (Equation 1).

$$\delta^2H = 8\ \delta^{18}O + 10‰\ SMOW \quad \text{(Craig, 1961)} \qquad (1)$$

These waters plot along what Craig defined as a Global Meteoric Water Line (GMWL), which has a slope 8 (Figure 8). The scientific breakthrough would allow for the correlation of meteoric water on a global scale.

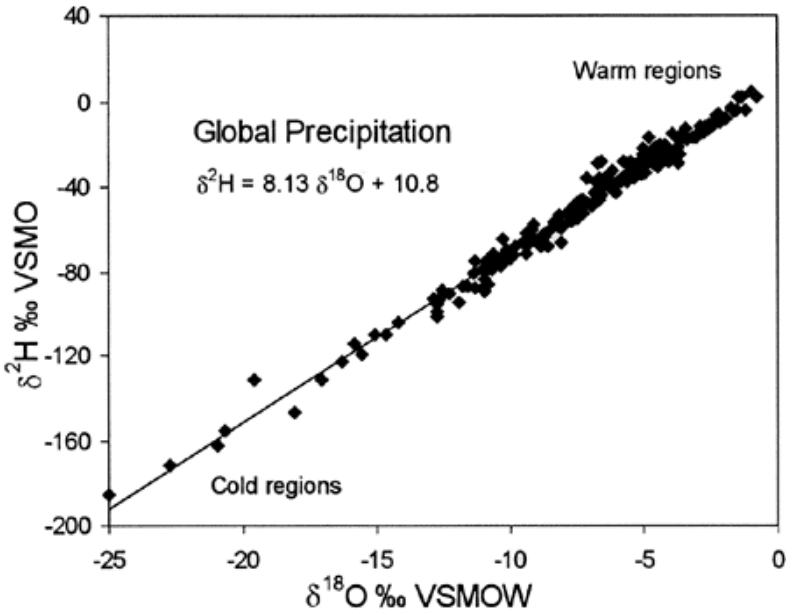

Figure 8. Relationship between $\delta^{18}O$ and δD in meteoric water. Values in per-mil with respect to VSMOW. (From Clark and Fritz 1997, as compiled in Rozanski et al. 1993).

The difference in mass that exists between isotopes leads to isotope fractionation (Clark and Fritz, 1997). Because this process is thermodynamically driven, fractionation will occur at different rates for different air temperatures (Clark and Fritz, 1997). Understanding and interpreting these rates is the basis for using $\delta^{18}O$ and δD as groundwater tracers.

Although the relationship between isotope fractionation and temperature was first discovered in 1947 by Harold Urey (Equation 2), it wasn't until 1961 when the predictability and correlation between the two components was discovered, which became the foundation for isotope hydrology (Figure 8).

$$\mathbf{Q = \sigma m^{3/2} \Sigma e^{-E/kT}} \quad (2)$$

Q = bond strength or dissociation energy (kJ/mol) σ = a symmetry value

T = thermodynamic temperature (K) m = mass (kg)

E = the energy state ($J \cdot mole^{-1}$)

K = Boltzmann constant = $n \cdot 1.380658 \cdot 10^{-23}$ JK^{-1}

For water samples, oxygen and hydrogen isotopes are measured and expressed as ratios between the two most abundant isotopes (e.g. $^{18}O/^{16}O$). This ratio is "normalized" by a reference sample (i.e. Standard Mean Ocean Water (SMOW)) (Equation 3), which was determined by Craig [1961]. Isotopic values are expressed using the delta (δ) notation (Equation 3). Because fractionation between the reference and sample is usually small, results are expressed in per-mil (‰) (Clark and Fritz, 1997).

Note: Since Craig, the reference has been slightly modified to VSMOW (V for Vienna), which is used today (Clark and Fritz, 1997).

$$\delta^{18}O_{sample} = \left(\frac{(^{18}O/^{16}O)_{sample}}{(^{18}O/^{16}O)_{reference}} - 1 \right) \cdot 1000 \quad (3)$$

One of Craig's key observations for meteoric water was the relationship between temperature and isotope ratios in precipitation (Figure 8). A few years later, Dansgaard [1964] established a linear relationship between temperature and $\delta^{18}O$ (Equation 4).

$$\delta^{18}O = 0.695\ T(^{o}C)_{\ annual} - 13.6\ ‰\ SMOW \quad (4)$$

Clark and Fritz [1997] discuss the strong correlation between temperature and $\delta^{18}O$ in meteoric waters, and provide examples of a variety of physiographic variations (e.g., altitude, latitude, land mass etc.) which influence temperature, and therefore influence the isotopic composition of precipitation.

Altitude Effect

In regions with topographic relief, lower temperatures are typically consistent with higher altitudes. Precipitation within the colder region will be depleted in heavy isotopes when compared to nearby rain samples from lower (i.e. warmer) elevations. Applying this criterion, it is possible to determine elevations (and areas) of recharge. Eastoe et al., [2004] were able to distinguish between mountain and basin precipitation from groundwater samples using $\delta^{18}O$ and δD.

Physiographic conditions such as elevation can influence the isotopic composition of precipitation, providing a tool for identifying sources of recharge. The influence that elevation, has on $\delta^{18}O$ is known as an "altitude effect" (Figure 9). This effect is typically measured as a rate of depletion of $\delta^{18}O$ due to a rise in elevation. The gradient typically ranges from 0.15 to 0.5‰ $\delta^{18}O$ depletion per 100-meter rise (Clark and Fritz, 1997).

Watersheds with significant topographic relief may therefore display considerable variation in $\delta^{18}O$ and δD. However, a $\delta^{18}O$ depletion rate for the area must be well-known to help determine accurate elevations of recharge.

Rainout Effect

Another useful isotopic tracer in groundwater recharge studies is the "rainout effect". This effect does not primarily rely on a temperature gradient, but rather on the progression of a storm. As a vapor mass (i.e. cloud) cools adiabatically, and exceeds its dew point, precipitation will occur. Over the course of the storm, the isotopic composition of the liquid

phase (i.e. precipitation) will become depleted in heavy isotopes. This phenomena, known as the "rainout effect", can be described using a Rayleigh-type distillation ($R = R_o f^{(a-1)}$), where: Ro= initial isotope ratio; R= ratio after the process occurs; *f*= residual component; a= equilibrium fractionation factor (Figure 10) (Clark and Fritz, 1997).

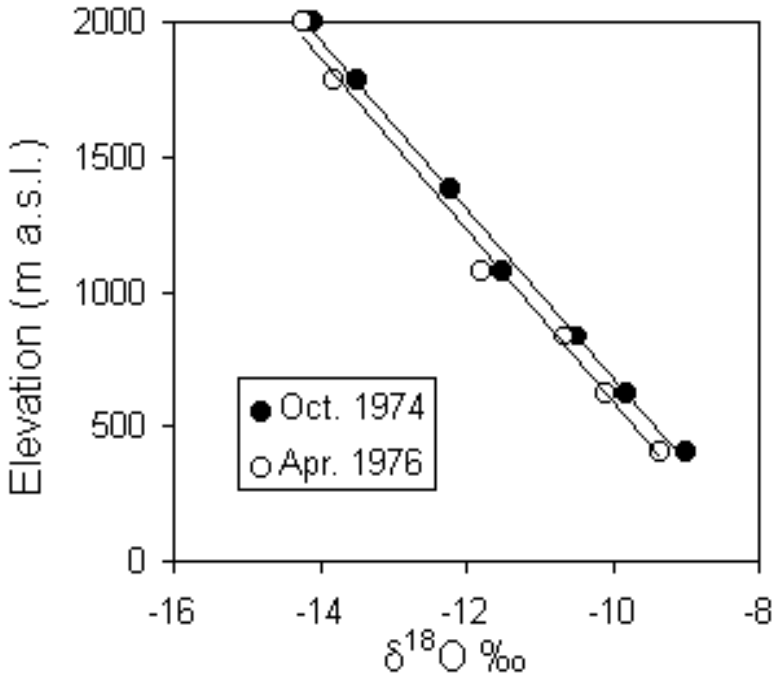

Figure 9. Altitude correlation (i.e. altitude effect) in $\delta^{18}O$. As elevation increases, $\delta^{18}O$ becomes increasingly depleted (-0.31 ‰ $\delta^{18}O$ per 100-m rise in elevation). (Clark and Fritz, 1979, taken from Bortolami, 1979).

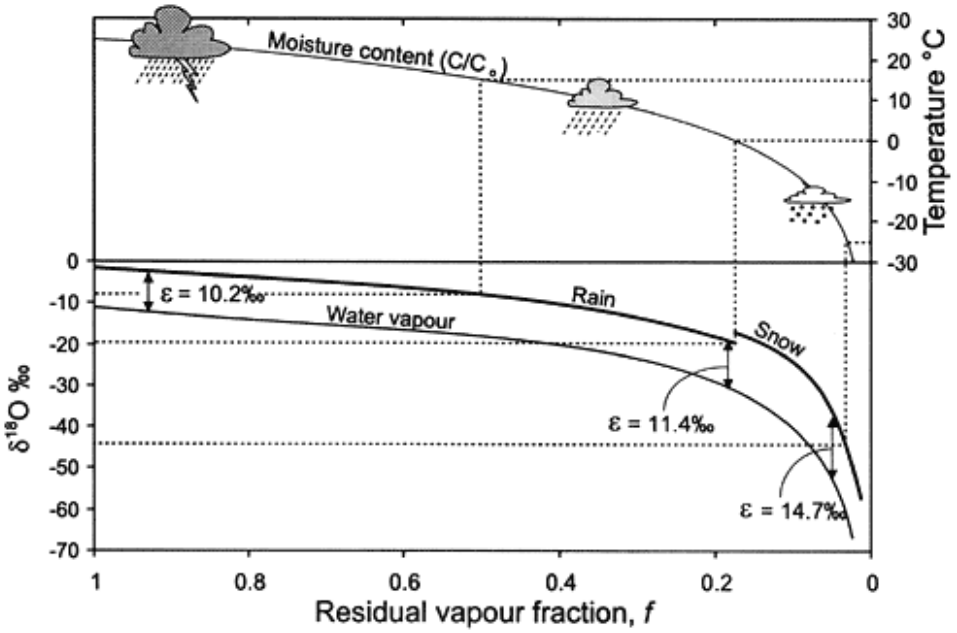

Figure 10. Change in ^{18}O of precipitation according to a Rayleigh distillation (Clark and Fritz, 1997).

Figure 11, which displays a "rainout effect", shows an original vapor mass of -12‰ $\delta^{18}O$ moving on-land. The first precipitation event releases the heavier isotopes, leaving the residual vapor mass depleted in $\delta^{18}O$ (-15 ‰). As precipitation continues, the residual vapor mass becomes increasingly depleted in $\delta^{18}O$.

When a vapor mass moves across a continent with significantly cooler temperatures (known as a *continental effect*), the isotopic composition of precipitation may display extreme depletion in heavy isotopes. Coastal regions with nearby mountains may show this effect (Figure 12) (Clark and Fritz, 1997).

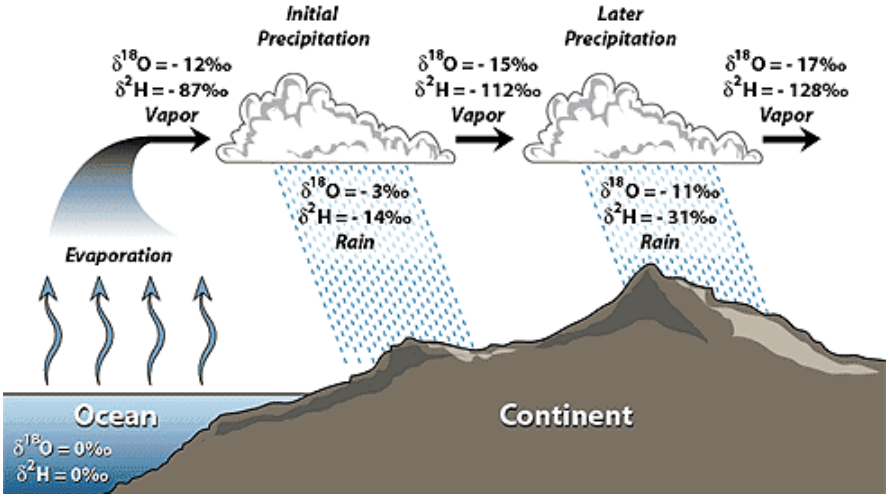

Figure 11. Schematic diagram displaying the "rainout effect" on $\delta^{18}O$ and δD (From SAHRA webpage, based on Hoefs, 1997 and Coplen et al., 2000).

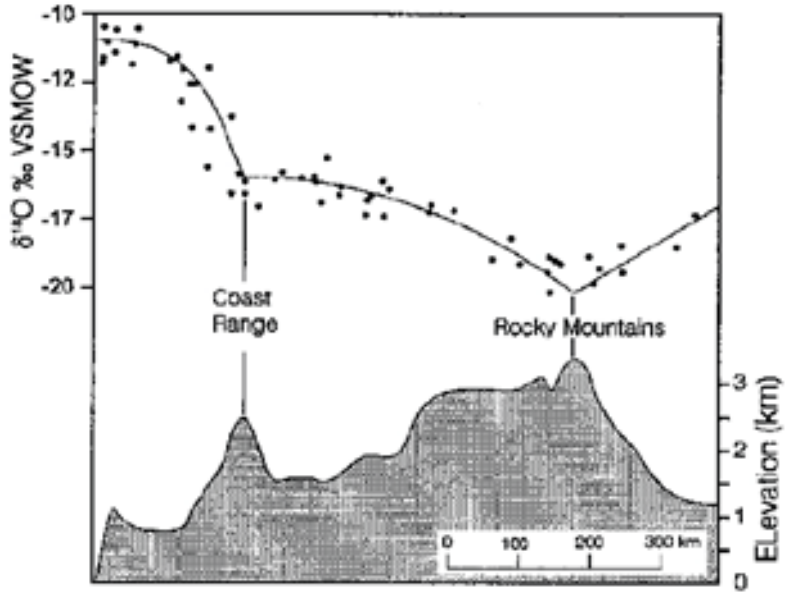

Figure 12. $\delta^{18}O$ effect of precipitation across a continental landmass. The factors controlling the depletion of heavy isotopes are a combination of temperature and rainout effect (Clark and Fritz, modified from Yonge el al., 1989).

Evaporation Effect

Stable isotope data can also be used to determine the degree of evaporation a water sample has undergone. These results can be used with additional data to help determine the time and type of infiltration occurring within a watershed.

Evaporation will occur depending on the temperature, humidity, and time it takes water to infiltrate to a point where it is no longer affected by elevated temperatures. In arid and semi-arid regions, groundwater often shows indications of evaporation. $\delta^{18}O$ and δD data can help determine whether this highly fractionating process is occurring (Clark and Fritz, 1997).

Evaporation of water is recognized by an enrichment of $H_2{}^{18}O$, which can be explained by the difference in vapor pressure between ^{18}O and ^{16}O (Equations 5 and 6) (Clark and Fritz, 1997), where Je = evaporative flux.

$$\textbf{REACTION 1: } \mathbf{H_2{}^{16}O_{(liquid)} \xrightarrow{Je} H_2{}^{16}O_{(vapor)}} \quad (5)$$

$$\textbf{REACTION 2: } \mathbf{H_2{}^{18}O_{(liquid)} \xrightarrow{Je} H_2{}^{18}O_{(vapor)}} \quad (6)$$

Based on the differences in bond strength between the two reactions, reaction 1 will proceed 1% faster than reaction 2, at 20°C (Szapiro and Steckel, 1967).

This increase in vapor pressure leads to enrichment of ^{16}O in the vapor phase and enrichment of ^{18}O in the liquid phase. Therefore, evaporated samples plot to the right of the Global Meteoric Water Line (GMWL) (Clark and Fritz, 1997).

Evaporation effects on $\delta^{18}O$ and δD may provide insight into the type of recharge occurring for an area. For example, highly evaporated waters may indicate a *diffuse*-type of recharge, where water is prone to elevated temperatures during infiltration (Sukhija et al., 2005; Clark and Fritz, 1997). If groundwater samples show no sign of evaporation it may indicate rapid infiltration, possibly from *focused* flow in fractures with little or no soil. Sediment

grain size can also contribute to the degree of evaporation effects, where fine-grained sediment may lead to greater evaporation effects than course-grained sediment, as seen in a study by Eastoe et al., [2008].

The degree of isotopic enrichment (i.e. evaporation) can be determined from the slope of the evaporation line, which typically varies between about 3 and 5, depending on relative humidity (Figure 13). Slopes near 3 are typical for regions where recharge occurs when humidity approaches 0. A Slope near 5 is typical when recharge occurs in 75% relative humidity (Clark and Fritz, 1997). Water undergoing continuous evaporation will continue to be enriched in heavy isotopes. If the evaporation slope is known, the evaporated samples can be "traced" back to their isotopic origin (Clark and Fritz, 1997). Knowledge of the evaporation slope and an understanding of infiltration process can significantly help understand recharge in arid and semi-arid regions.

Aside from evaporation, many factors control the isotopic composition of water, as explained throughout this section. Figure 13 shows many of the trends associated with fractionation under different physiographic conditions.

Paleoclimate Effect

Temperature in temperate latitude climates has greatly varied since late Pleistocene time (Clark and Fritz, 1997). Due to the strong correlation between temperature and $\delta^{18}O$, precipitation from different periods (with different temperatures) can be characterized by having distinct isotopic ratios from modern precipitation (Siegel, 1991; Eastoe et al., 2008; Clark and Fritz, 1997). Depleted $\delta^{18}O$ values have been shown to be from colder precipitation (e.g., late Pleistocene precipitation) (Darling et al., 1998; Clark and Fritz, 1997).

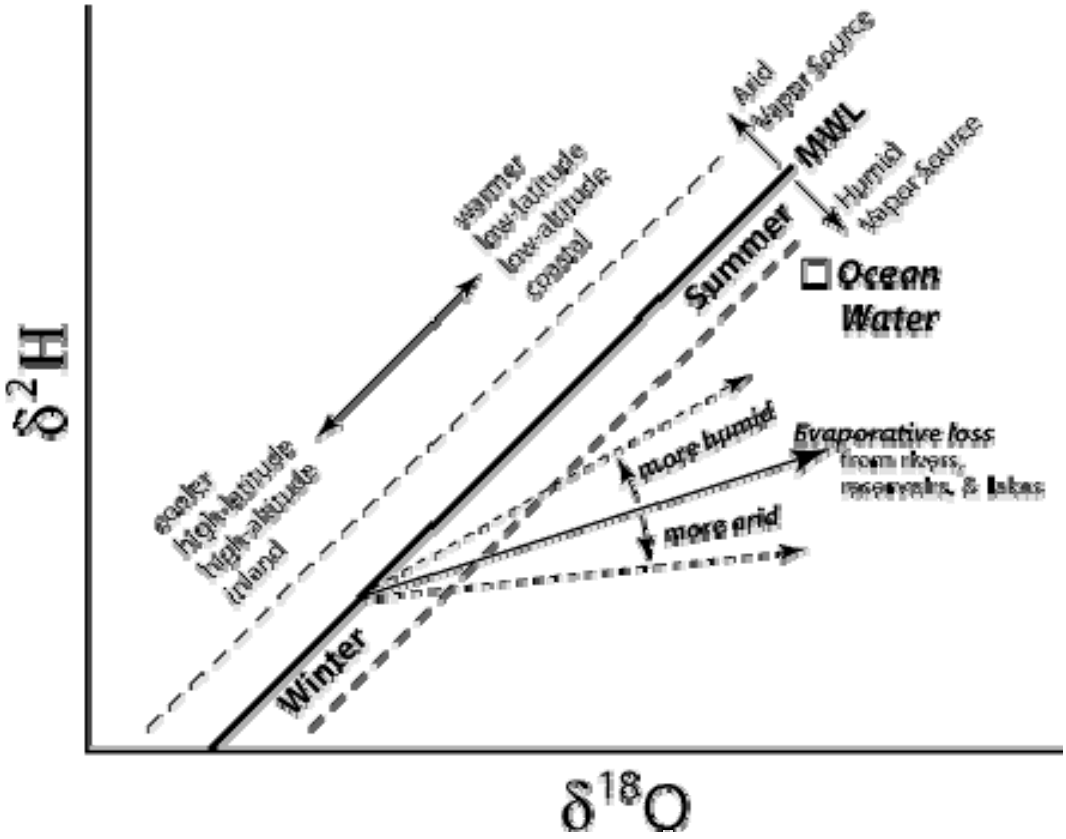

Figure 13. Many of the physical conditions which cause $\delta^{18}O$ and δD fractionation. Note the slopes of the evaporation lines are much lower (or smaller) than the MWL, which has a slope of 8 (from SAHRA webpage).

I.6 Tritium

Water samples are commonly tested for the radioactive isotope tritium (^3H) to help identify the existence of modern (past few decades) recharge (Clark and Fritz, 1997). The basis for using tritium as a groundwater dating technique began in 1951 when thermonuclear bomb tests began "leaking" tritium into the atmosphere (Figure 14). A ^3H maximum was reached in 1963, and ^3H was effectively exhausted from the atmosphere in 1992 (Clark and Fritz, 1997; Eastoe, personal communication, 2009). Because precipitation acquires the atmospheric concentration of tritium, present-day analyses use this ^3H peak as a reference to determine at what time the sample (i.e. groundwater) was in contact with the

atmosphere. Due to the criterion used, tritium analyses do not provide 'age" information prior to 1952.

Tritium's half-life is 12.43 years, and is measured in TU (tritium units), where 1 TU equals 1 ^{3}H per 10^{18} hydrogen atoms (Michel, 2005). Tritium concentrations in natural waters are directly related with the "age" (i.e. residence time) of the water (Clark and Fritz, 1997).

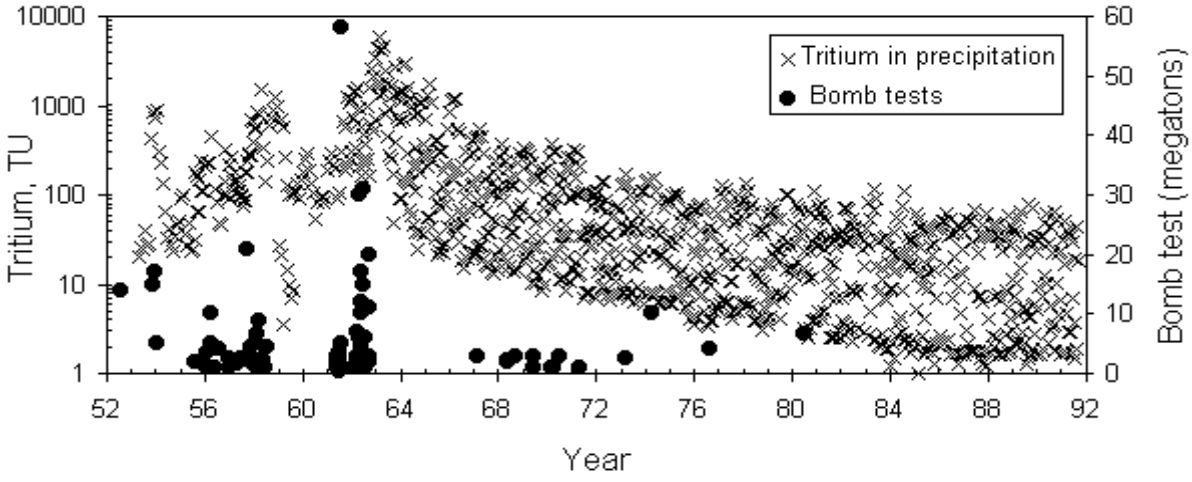

Figure 14. Tritium in precipitation from thermonuclear bomb tests from 1952-1992. Based on data from North America and Europe. Data from International Atomic Energy Agency (IAEA) and Global Network of Isotopes in Precipitation (GNIP).

II. MATERIALS AND METHODS

II.1 Meteorological Data

Meteorological Station Data

Two meteorological stations operated by the National Water Commission (CONAGUA) exist within the Santo Tomás watershed: the Santo Tomás (#2065) and the El Álamo (#2014) stations. Both stations contain daily meteorological data, which were used to calculate monthly and annual (September – August) average precipitation and pan evaporation. Data exist from 1948–2002 for the Santo Tomás station and from 1961–1994 for the El Álamo station. However, due to missing data, only 26 of the most reliable years were used (1962-1988).

II.2 Basin Characterization

Topography

Prior to fieldwork, a topographic map of northwest Baja California was created in ArcGIS 9.2, particularly using the Spatial Analyst extension and the Hydrology Toolbox. A 90 meter-resolution digital elevation model (DEM), downloaded in September 2008 from the CGIAR-CSI homepage (http://srtm.csi.cgiar.org/) and projected in UTM (WGS 1984) coordinates, was used to delineate the watershed of interest. Additionally, the watershed was also obtained by hand using 1:50000 INEGI topographic maps.

Lithology

A 1:250,000 geologic map (Gastil, 1975) was used as reference for the rock types within the study area. A map demonstrating the lithology within the watershed was generated in ArcGIS 9.2.

Normalized Difference Vegetation Index (NDVI)

A normalized difference vegetation index (NDVI) was derived to determine areas within the watershed containing live green vegetation. The NDVI, which is a ratio using the red and near-infrared bands (NIR) (Equation 7) from the electromagnetic spectrum, ranges between -1 and +1, and is used to differentiate between areas with green vegetation and non-vegetated areas (Morawitz et al., 2006).

$$\mathbf{NDVI = (NIR - Red) / (NIR + Red)} \quad (7)$$

Red and NIR bands from an October 8, 2008 Landsat Thematic image (Landsat-7 mission) of the study area were downloaded from: (http://glovis.usgs.gov/), and used in ArcMap 9.2 to derive NDVI. The images were from a relatively dry month to help determine areas with year-round vegetation, which could be attributed to springs or shallow water tables.

Negative NDVI (approaching -1) typically correspond to water, whereas values near zero (-0.1 – 0.1) relate to dry vegetation, bare soil, or barren areas of rock. Values from 0.2 to 0.4 generally account for shrub and grassland (Morawitz et al., 2006), and high values (> 0.4), typically correspond to live plants (Smith el at., 2006).

Fracture-Trace Map

Stereo-paired aerial photography (1:25,000) and Google Earth imagery (earth.google.com/, last accessed in June 2009) were used to create a fracture-trace map of the watershed. The lineaments mapped for this study represent any obvious linear feature within the watershed, including: vegetation trends, soil tones, fractures, faults etc. Field work consisted of examining lineaments, previously determined from photo-interpretation, for geomorphic evidence of active faulting, such as fault scarps, offset drainages, beheaded drainages etc.

II.3 Water Sampling

Water samples were taken between October 2008 and May 2009. In total, 20 sites were sampled, including: 11 natural springs, 3 wells, 2 small ponds, and multiple stream samples along the Santo Tomás arroyo. In addition, one rain sample was collected following a storm in December 2009, using a Clear Vu™ rain gauge. All spring samples and both pond samples were taken during a dry month (October 2008). The stream samples and one well sample were taken during both the wet and dry seasons.

Springs were sampled at their discharge point to minimize atmospheric contamination. For low-flowing springs, hand-made weirs were built to promote water circulation.

The three wells are hand-dug, each ~2 m in diameter. A submersible pump with 3/4"tubing was used to purge each well for 15 minutes prior to sampling.

Stream samples from the arroyo were taken in an area with rapid flow, usually near the center of the streambed.

1.5 liters were sampled from each site, and stored in polyurethane bottles. All bottles were filled quickly and completely, leaving minimal air space. Bottles used for hydrochemical analyses were pre-rinsed in hydrochloric acid; all bottles were pre-rinsed in distilled water. Samples were stored in an ice chest, and later transferred to a refrigerator at the hydrochemistry laboratory at the Center for Scientific Research and Higher Education (CICESE).

Temperature and electrical conductivity (EC) were measured in the field for most samples, using a thermometer and an electrical conductivity meter. A GPS fix was recorded for each site as well.

II. 4 Hydrochemistry Analysis (Cations and Anions)

Cation and anion analyses were completed in the hydrochemistry laboratory at CICESE. Procedure for bicarbonate detection was completed in the lab shortly after sampling, which consisted of titrating 40 ml of each unfiltered sample with 1 Molar HCl to a pH of 4.3.
Prior to analyzing cations and anions, the samples were filtered using a 0.5 um membrane filter, and placed in 100 ml bottles. Additionally, cation samples were lowered to pH < 2 by nitric acid addition, to avoid any precipitation of metals.

Anion analyses were performed for each sample using a Dionex IC 2000 ion chromatograph equipped with an SRS 300 surpressorass spectrometer. The major ions obtained include: Cl^-, F^-, Br^-, NO_3^-, PO_4^{3-}, NO_2^-, SO_4^{2-}.

Cation analyses were completed in the CICESE laboratory using a Varian Liberty 100 ICP-OES spectrometer. The major ions obtained include: Na^+, Ca^{2+}, Mg^{2+}, K^+, and Si.

A Na vs. Cl graph was plotted in Excel, and a piper diagram was generated using Rockware software (Rockworks 2006).

II. 5 Stable Isotope Analysis ($\delta^{18}O$, δD)

50 ml of each sample was collected and sent to the Environmental Isotope Laboratory at the University of Arizona for $\delta^{18}O$ and δD analyses. Isotopes were measured with respect to Vienna Standard Mean Ocean Water (VSMOW) using a Gas Source: Isotope Ratio Mass Spectrometry (IRMS). Results were graphed as x, y plots in Excel.

II.6 Tritium Sampling and Analysis

One hot spring and one cold spring were sampled for tritium (^3H) concentrations. Each sample was collected near the spring's origin, and underwater, to avoid contamination with present-day atmospheric tritium. Wristwatches were not worn during collection due to certain luminescent watches which contain tritium, and could contaminate the samples. The 2 samples were collected in January using pre-rinsed 500 ml polyurethane bottles and analyzed at the University of Arizona, using liquid scintillation counting (LSC). The method used was limited to <0.6 TU detection.

II. 7 Thermal Spring Discharge

The discharge of the dominant thermal spring (Figure 15) was measured on 8 occasions, from November 2008 to August 2009, approximately once per month. Measurements consisted of recording the time to fill a 17-liter bucket, and calculating the discharge in liters per second. On each of the 8 occasions, 5-10 measurements were made, and an average discharge was recorded.

In addition, on December 19-20, 2008, a measurement was taken at 3 hour intervals from 11am to 1am. In total, 5 measurements were recorded.

The spring was measured to observe the fluctuation of discharge throughout the year, and to determine if the thermal system responded to changes of precipitation throughout the season.

Figure 15. Discharge of the dominant thermal spring.

RESULTS

III.1 Meteorological Data

Annual precipitation (September – August) was calculated using daily rainfall data from (1962-1988) for the Santo Tomás and El Álamo stations (Figure 16). The Santo Tomás station averaged 286 mm/yr., and the El Álamo station averaged 347 mm/yr.

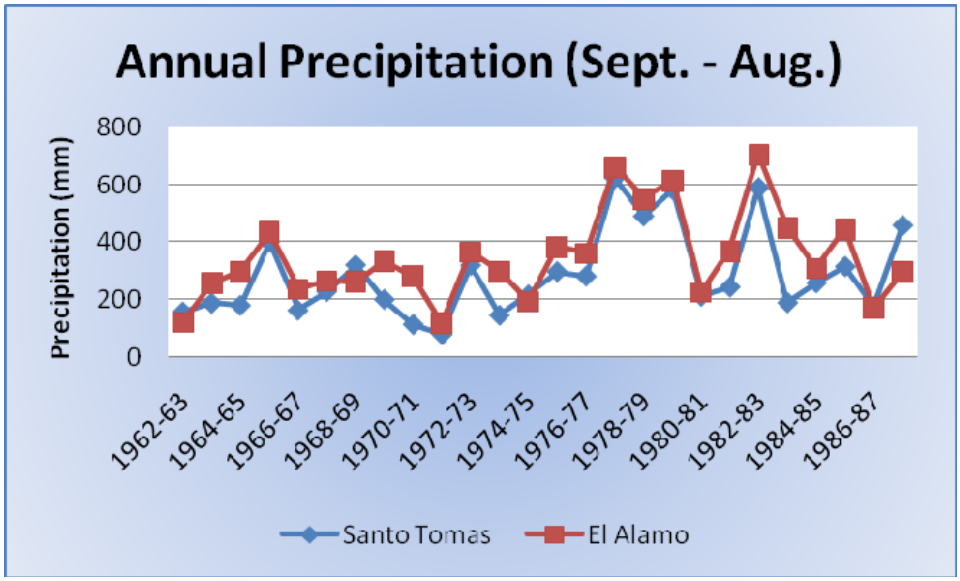

Figure 16. Annual precipitation (September – August) from 1962-63 to 1987-88 for both the Santo Tomás (station #2065) and El Álamo (station #2014) weather stations. Data obtained from the Comisión Nacional del Agua (CONAGUA).

Based on the 1962–1988 data, the El Álamo station averages slightly more annual rainfall from October to June, and significantly more during the monsoon season (July to September) (Table I). These monsoonal thunderstorms are not elevation-driven, but rather geographically influenced. They typically come up from the Gulf of California and have a greater effect on the eastern half of the Baja California Peninsula. Figure 17 displays examples of two years in which the monsoonal storms have a greater affect on the El Álamo station.

Table I. Average precipitation from October – June and July – September from 1962-88 for both the El Álamo and Santo Tomás weather stations. July – September corresponds to the monsoon precipitation (Data from CONAGUA).

	Avg. Precipitation *October – June* (1962-1988)	**Avg. Precipitation *July – September* (1962-1988)**
Santo Tomás	**276 mm**	**10 mm**
El Álamo	**272 mm**	**75 mm**

Results shown here differ from CONAGUA [2008], who report 200 mm/yr. The differing results most likely represent data from different periods.

Pan evaporation data from the Santo Tomás station were also analyzed. Monthly comparisons between precipitation and pan evaporation can be used to demonstrate the relative aridity for the region, as well as give insight into the probability of recharge for the region. Based on data from 1962-1988, approximately 9 of the 26 years display (visually) seasons in which monthly precipitation exceeds monthly pan evaporation. In general, these years are considered "wet", whereas in "dry" years, pan evaporation exceeds precipitation for most or all of the months. Nevertheless, pan evaporation (class A) has been shown to overestimate actual evaporation from a lake surface by up to 25% (Charles-Edwards and O'Keeffe, 2003).

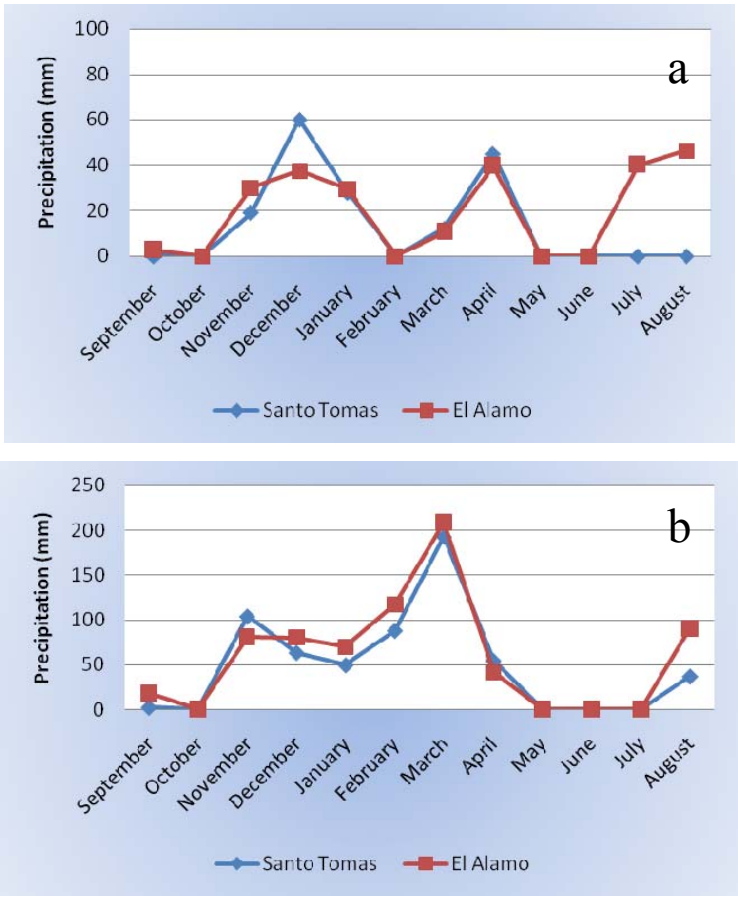

Figure 17. Two examples of annual precipitation for the Santo Tomás and El Álamo weather stations from a) 1966-67 and b) 1982-83. From October – May the stations receive similar amounts of precipitation. However, in July, August and September, the El Álamo station received greater amounts of rainfall from the monsoon storms. Data from CONAGUA.

Figure 18(a) shows an example of a year when pan evaporation exceeded precipitation throughout the year. However, this result is based on monthly values; daily or weekly storm events typically exceed pan evaporation, which may result in groundwater recharge. The factor controlling recharge under these conditions is the time it takes water to infiltrate to a point where it is no longer affected by evaporation. Rapid infiltration in faults and fractures may recharge the aquifer regardless of the elevated evaporation rates, whereas water in dry soil or sediment may need weeks or months to infiltrate through the vadose zone. The slow infiltration rates may result in negligible recharge for the years experiencing this dry trend.

An example of a wet year is displayed in Figure 18(b); precipitation exceeds pan evaporation for multiple months. Increased recharge can be expected during such years, especially in areas of the basin with thicker soils or sediment (e.g. flat surfaces, streambeds, etc.). Channel recharge (a *focused* mountain-*front* component) becomes increasingly important during wet years.

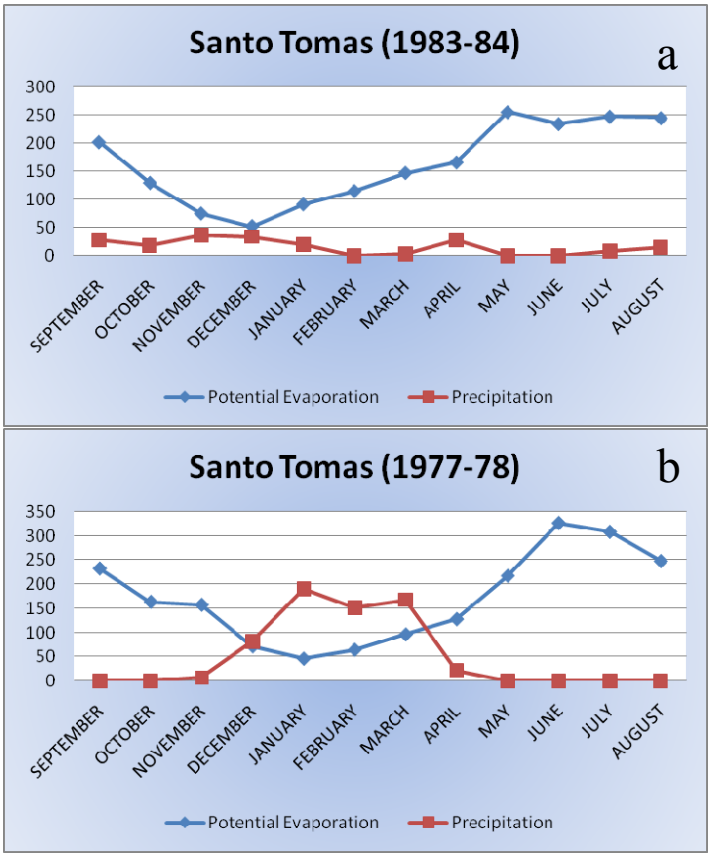

Figure 18. Examples of the possible monthly relationship between precipitation and pan evaporation at the Santo Tomás weather station. a) During the "dry" year (1983-84) pan evaporation exceeds precipitation throughout the entire season, which in theory, would indicate no groundwater recharge. b) However, the "wet" year (1977-78) shows a 3 to 4 month period where precipitation exceeds potential evaporation. Based on the 26-year time series used to compare these parameters, approximately 9 out of 26 years display precipitation exceeding pan evaporation for a full year.

III. 2 Basin Characterization

To characterize the watershed physically, maps of *elevation, slope, lithology, NDVI*, and *fractures* for the study area (~300 km^2) were created. Each map was examined individually as well as in conjunction with other physical and chemical parameters to understand the dynamic of the watershed.

Topography

Elevation data from Figure 3 were used to estimate the mean, maximum and minimum elevations for the study area (Table II). Slope was also estimated (Figure 19) using these data to help visualize the topography.

Table II. Elevation data in meters above sea-level (m.a.s.l.) for the Santo Tomás eastern sub-watershed. Data from 90-m DEM.

Elevation of Watershed (~300 km^2)	
Minimum Elevation	285 m.a.s.l.
Maximum Elevation	1660 m.a.s.l.
Range in Elevation	1375 m.a.s.l.
Mean Elevation	1038 m.a.s.l.

Slopes within the watershed range from 0-46 degrees, with the steepest gradients concentrated along the Santo Tomás arroyo. Steep slopes (20 – 30 degrees) along the arroyo are consistent with water erosion caused by runoff from storm events. Slopes above the angle of repose (30 degrees) will "erode" by collapse, and are likely to be hard rock areas. The easternmost section of the watershed, near the town of El Álamo, consists of terrain with low or 0 slope, which will favor infiltration. Although the ill-defined watershed boundary terminates on this approximately planar surface, this flat area extends for ~15 km east of El Álamo, to the foothills of the Sierra Juárez and San Pedro Mártir mountains.

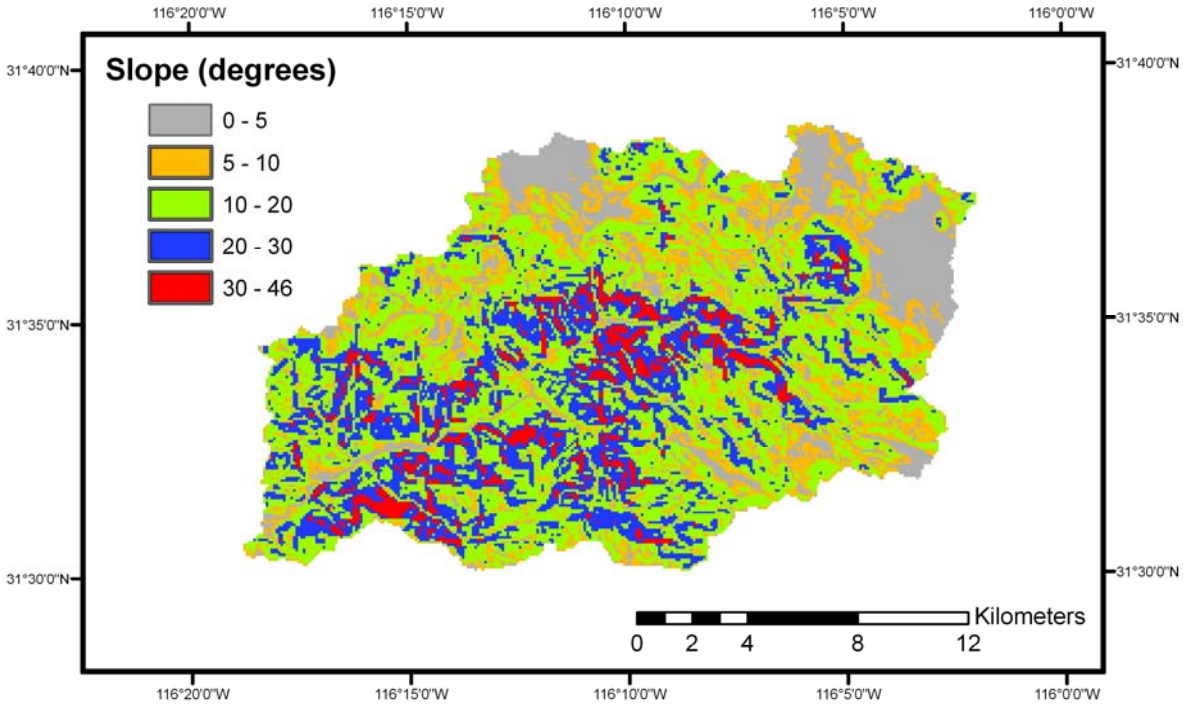

Figure 19. The Santo Tomás eastern sub-watershed showing the slope of terrain in degrees. Steep areas around the Santo Tomás arroyo reach slopes of 46°. The eastern section of the study area (El Álamo) is relatively level or flat, consisting of slopes near or of 0. Data based on 90-m DEM.

Geology (lithology)

Aside from Quaternary alluvium along the Santo Tomás valley, most rocks are from the Mesozoic Era, associated with subduction of the ancient Farallon plate (Gastil, 1975). Pre-batholithic and batholithic rocks within the study area form part of the Peninsular Ranges, and include: granitic rock (undifferentiated), granodiorite, gabbro, gneiss and andesite (Gastil, 1975) (Figure 20). The volcanic rock (andesite) is heavily fractured. This result is likely due to brittle deformation associated with the Agua Blanca fault, which cuts across the rock. Granitic rock is found throughout the study area, and is also heavily fractured.

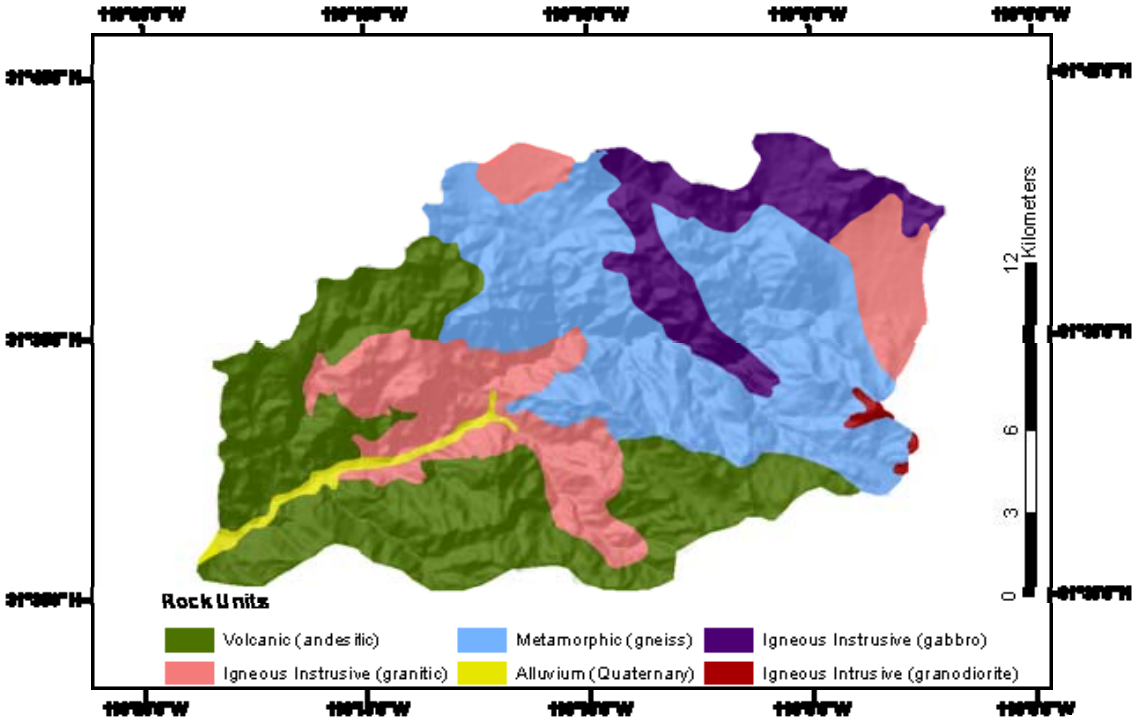

Figure 20. Lithology of the Santo Tomás eastern sub-watershed. Aside from alluvium, the watershed consists of volcanic and plutonic rock, both of which have negligible primary porosities (map created using Gastil, 1975).

Vegetation (NDVI)

NDVI for the study area range from -0.15 to 0.6. The lowest NDVI (-0.15 – 0.1, denoted by the color grey in Figure 21) are seen along the length of the Santo Tomás arroyo, and most likely represent barren areas of rock. Extensive areas with high NDVI, such as the "southern section" and "southeast section", contain values between (0.2 – 0.6, denoted by blue and red in Figure 21). These specified, vegetated areas are north-facing slopes near the peaks of mountain-tops.

Near the middle of the watershed, a small area displaying high NDVI (seen as a linear series of red and blue dots) can be seen within an area of predominately low NDVI (grey area) (Figure 21). This section, labeled "proximal to the thermal springs", coincides with a 5 km stretch of the Santo Tomás arroyo, where thermal spring discharge flows year-round. This area consists of live green vegetation adjacent to barren areas of rock, and can be

associated with active faulting and spring water. This result might be useful in locating springs and/or active faults.

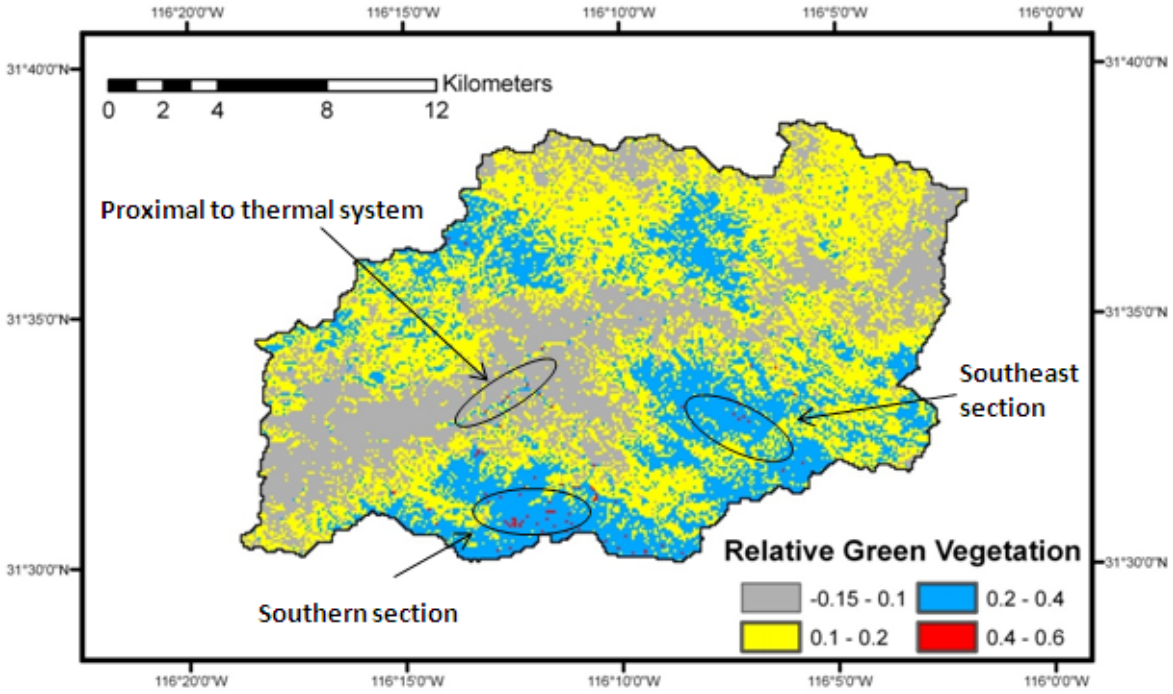

Figure 21. Normalized Difference Vegetation Index (NDVI) map of the Santo Tomás eastern sub-watershed showing relative green land cover in October 2008. Based on Landsat image from USGS GloVis from October, 2008. The image used was from a relatively dry month with the intention to locate year-round flowing springs.

Fracture-Trace Map

Lineaments within the watershed are oriented mostly ~N50W – N70W, which is consistent with the strike direction of the dominant fault in the area (i.e. Agua Blanca). Multiple lineaments were also observed for most of the length of the arroyo, which were oriented ~N60E (Figure 22).

Aside from a strand of the Agua Blanca fault (shown in dark red) near the south-west tip of the study area, only one lineament displayed active tectonic geomorphic features. This lineament, located near the middle of the watershed, passes within meters of the hot spring system, and appears to be an active fault. Striking approximately N50W and displacing

multiple small stream channels, its dextral-sense of motion can be traced for most of its 3 km length.

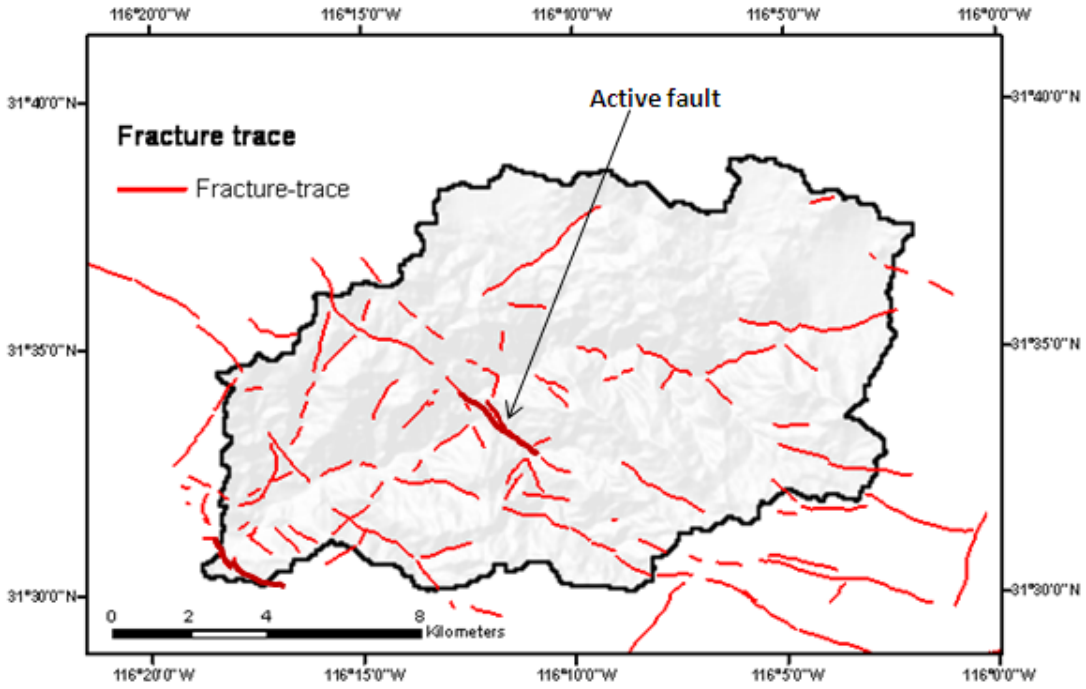

Figure 22. Fracture-trace map of the Santo Tomás eastern sub-watershed showing significant lineaments within and adjacent to the study area. Lineaments, traced using aerial photographs (1:25000) and Google Earth, represent many types of physical features, including vegetation trends, soil tones, fractures, faults etc.

III. 3 Water Sampling

Geographic coordinates and elevation for each of the 21 water samples collected throughout the study area are presented in Table III. The "name" for each sample is used for reference only. Figure 23 shows the locations for each of the sites within the Santo Tomás eastern sub-watershed. Most of the samples were collected in steep terrain, along the Santo Tomás arroyo, where elevations ranged from 315 – 642 meters above sea level (m.a.s.l.). One sample ("El Álamo" #14) was collected along the flat, eastern section of the watershed at 1114 m.a.s.l. The rain sample (#21) was collected near site #10 at approx. 520 m elevation. A cold spring (#4) was sampled just beyond the watershed boundary (in the

southwest corner) because I consider it representative for the watershed and helpful to the study.

Note: Sample #3 is not a thermal spring; its temperature at surface is ambient. However, it is located ~50 m from the dominant thermal spring, and based on isotope and hydrochemistry data, sample #3 has been shown to originate from the same source as the other two thermal springs (#1 and 2). Therefore, to simplify the data, we consider this sample of thermal spring origin. Aside from this exception, "Cold Springs" refer to all natural springs that display ambient temperature.

A comparison between spring locations and mapped lineaments show a direct relationship between the two. In particular, the two active faults in the study area are adjacent to multiple springs. Cold springs 4, 5 and 6 are located along the Agua Blanca fault. Springs 1, 2, 3, 10, 11 are located near the active fault in the lower portion of the watershed. Rock types do not appear to control spring location.

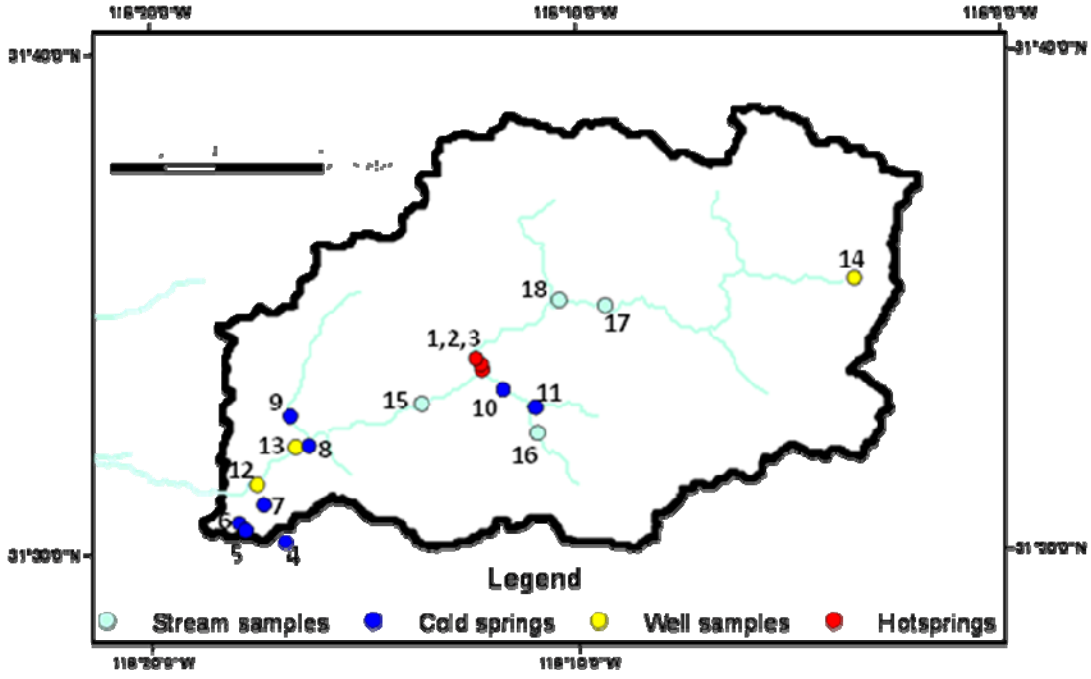

Figure 23. Locations of water samples taken during 2008 and 2009 for the study area.

Table III. Spring, well and stream samples. Flow was measured multiple times for sample 1. Note: the thermal springs and cold springs are located at similar elevation. The El Álamo well sample is located at 1114m, which is the highest elevation of all samples.

Sample Number	Type of Sample	Elevation (Meters)	Geographic Coordinates (latitude N/longitude W)	Name (Unofficial)
1	Thermal Spring	498	31°33'47.73 ; 116°12'13.81	AguaCaliente
2	Thermal Spring	483	31°33'40.20 ; 116°12'13.78	Warm Spring
3	Thermal Spring	495	31°33'48.41 ; 116°12'18.04	DiffuseWarm
4	Cold Spring	636	31°30'14.01 ; 116°16'51.56	Telnor
5	Cold Spring	426	31°30'27.23 ; 116°17'48.74	U-Turn
6	Cold Spring	400	31°30'37.54 ; 116°17'55.47	Ricardo
7	Cold Spring	550	31°30'58.13 ; 116°17'19.67	Ulises
8	Cold Spring	356	31°32'09.78 ; 116°16'18.46	Rigo
9	Cold Spring	394	31°32'45.17 ; 116°16'43.91	Rigo Canyon
10	Cold Spring	520	31°33'13.47 ; 116°11'39.96	Mark
11	Cold Spring	541	31°32'53.99 ; 116°10'57.74	Don Luis
12	Well	315	31°31'22.50 ; 116°17'30.97	Ulises
13	Well	358	31°32'08.38 ; 116°16'36.03	Rigo
14	Well	1112	31°35'26.00 ; 116°10'23.03	El Álamo
15	Stream	410	31°32'59.55 ; 116°13'39.83	Bronco
16	Stream	567	31°32'21.08 ; 116°10'54.05	Upstrm Mark
17	Stream	642	31°34'56.45 ; 116°09'17.34	El Salto
18	Stream	610	31°35'01.02 ; 116°10'23.03	DwnStr Salto
19	Pond	480	31°33'44.50 ; 116°12'10.64	Pond 1
20	Pond	480	31°33'50.16 ; 116°12'18.04	Pond2
21	Rain	520	31°33'23.54 ; 116°12'00.84	Rain

Results from field measurements, including: pH, electrical conductivity (EC) and temperature are presented in Table IV. “Flow” measurements for most of the natural springs were extremely difficult to determine due to their diffuse nature; therefore, most of the values are estimates.

Temperature was recorded for 8 of the samples; however, values from samples #5, 7, 18 and 19 may be high due to ambient temperatures. The temperature for the two hot springs (#1 and 2) was measured various times throughout the year; their temperatures remained fairly constant, varying less than 1 degree Celsius; the temperatures shown are their averages.

Total dissolved solids (TDS) for the samples range from 315 – 826 ppm, with the natural springs (cold and thermal) displaying the lowest concentrations. Upper-end TDS levels are found in stagnant water (samples # 18, 19, 20), and in the easternmost well sample (#14), which is a highly-used well, and is not stagnant.

Thermal springs (# 1 and 2) display high pH values (9.4); all other samples range in value between 7.0 and 8.3.

III. 4 Hydrochemistry (Cations and Anions)

Table V presents major cation and anion data for most of the samples collected within the study area. Significant differences between the thermal waters and all other samples are present in Ca, Mg, F and HCO_3. The thermal samples contain low concentrations of Ca (2.9 – 7.1 mg/l), Mg (0 – 1 mg/l) and HCO_3 (30 – 53 mg/l), when compared to all other samples; however, they contain much higher concentrations of F (5.2 – 11.6 mg/l).

Table IV. Results of pH, electrical conductivity (EC), total dissolved solids (TDS) and temperature for the 21 water samples. Flows < 1 liter/second are diffuse spring systems and are difficult to measure accurately.

Sample Number	Type of Sample	Flow l/s	pH	EC (ms)	TDS (ppm)	Temp. (^{0}C)	Name (Unofficial)
1	Thermal	~3	9.4	0.64	408	49.0	Agua Caliente
2	Thermal	~0.5	9.4	0.64	400	38.1	Warm Spring
3	Thermal	~0.05	7.0	0.62	397	-	Diffuse Warm
4	Cold Spring	~0.5	7.5	0.69	442	-	Telnor
5	Cold Spring	~0.1	7.2	0.95	608	24.8	U-Turn
6	Cold Spring	~0.05	7.9	0.63	403	-	Ricardo
7	Cold Spring	~0.25	7.7	0.83	531	28.1	Ulises
8	Cold Spring	~2	7.9	0.49	315	-	Rigo
9	Cold Spring	~2	7.5	0.61	390	-	Rigo Canyon
10	Cold Spring	~1.5	7.3	0.70	448	-	Mark
11	Cold Spring	~0.1	7.0	0.69	442	17.7	Don Luis
12	Well	n/a	7.0	0.75	480	-	Ulises
13	Well	n/a	7.8	0.85	544	-	Rigo
14	Well	n/a	7.6	1.28	819	-	El Álamo
15	Stream	n/a	7.9	0.92	588	-	Bronco
16	Stream	n/a	7.4	0.73	467	-	Upstrm Mark
17	Stream	n/a	7.6	0.79	506	21.9	El Salto
18	Stream	n/a	7.7	1.10	704	25.6	DwnStr Salto
19	Pond	n/a	7.3	1.29	826	26.9	Pond 1
20	Pond	n/a	8.3	1.20	766	28.3	Pond2
21	Rain	n/a	6.7	0.03	19	-	Rain

Table V. Table showing major cations and anions for 18 samples. Units are in mg/l. Where b/d is below detection.

Sample	Type	Ca	Na	Si	Mg	K	F	Cl	SO_4	HCO_3
1	Thermal	7.1	117.9	19.3	1.0	1.5	11.6	105	49	38
1	Thermal	6.1	97.0	18.8	0.0	0.9	5.3	100	47	30
2	Thermal	6.6	119.6	19.2	0.0	0.9	5.4	103	50	46
3	Thermal	2.9	94.4	17.2	0.26	1.0	5.2	96	46	53
4	Cold	65.9	48.8	14.3	19.6	bd	0.2	67	7	335
5	Cold	104.3	93.0	13.9	27.5	bd	0.2	174	21	376
6	Cold	59.7	59.3	13.3	17.1	bd	0.3	92	12	231
7	Cold	88.6	48.1	12.4	16.2	bd	0.0	163	25	223
8	Cold	42.5	32.5	12.8	16.0	2.4	0.1	46	19	152
9	Cold	66.3	58.2	16.3	16.0	bd	0.1	84	15	264
10	Cold	68.4	47.3	16.6	24.9	1.8	0.9	44	42	457
11	Cold	50.2	52.3	16.3	17.6	2.4	0.3	47	50	213
12	Well	64.7	71.6	13.8	19.8	1.5	0.6	90	55	244
12	Well	66.0	56.7	15.0	19.7	0.4	0.4	83	51	259
13	Well	82.3	62.8	14.9	24.4	2.8	0.2	107	46	274
14	Well	105.2	108.9	13.6	33.6	5.0	0.1	168	69	381
15	Stream	60.6	108.3	15.6	22.3	2.1	2.2	13	55	244
15	Stream	42.5	83.6	16.6	17.1	1.9	3.3	119	50	213
16	Stream	46.6	44.3	14.2	24.2	1.6	0.1	34	31	289
17	Stream	56.0	74.9	11.6	20.7	2.8	1.5	73	41	266
18	Stream	74.9	93.6	10.8	26.1	3.7	0.2	134	93	259
21	Rain	4.2	1.2	bd	1.0	bd	3.3	1.4	bd	15

A Na versus Cl graph of 19 samples show that most of the samples plot near the 1:1 ratio line (Figure 24); the thermal springs are slightly enriched in sodium. This enrichment could be indicative of increased thermodynamic interaction between the hot water and surrounding igneous rock, and can be associated with distinct water-rock interaction (Kretzschmar, personal communication, 2009).

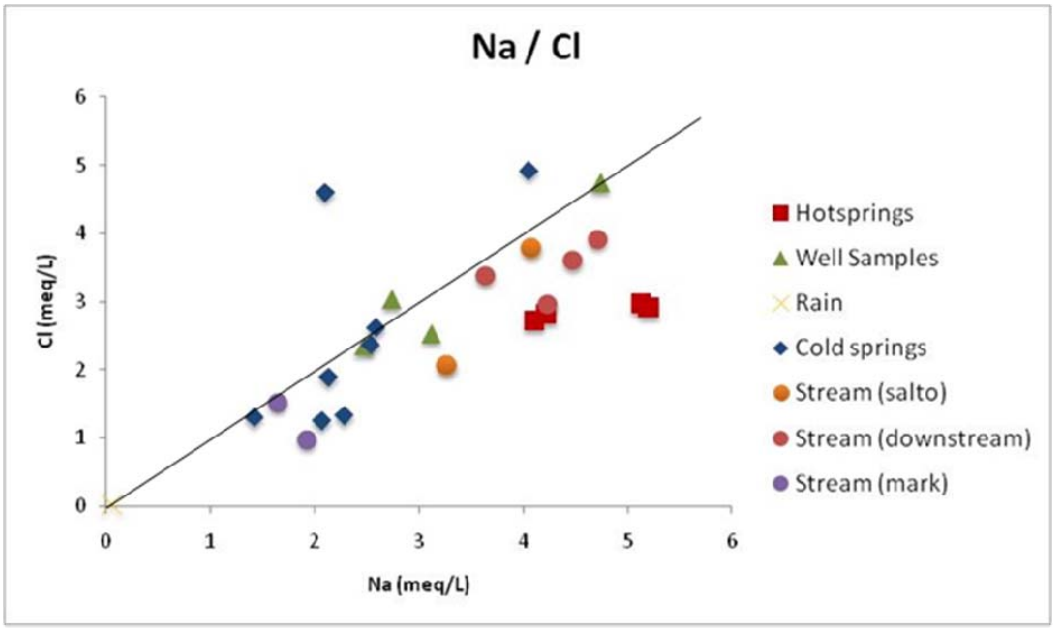

Figure 24. Plot of Na vs. Cl. with 1:1 line. Thermal springs are enriched in Na compared to cold springs.

A piper diagram was also generated using major cation and anion results for 19 of the 21 samples (excluding #19, 20) from the study area (Figure 25). Two distinct data are present: 1) thermal spring water, which can be classified as Na-Cl, and 2) all other samples, which do not display a dominate water type (i.e. mixed cations and anions). The two type of data suggest distinct water-rock interaction between the thermal springs and all other water,

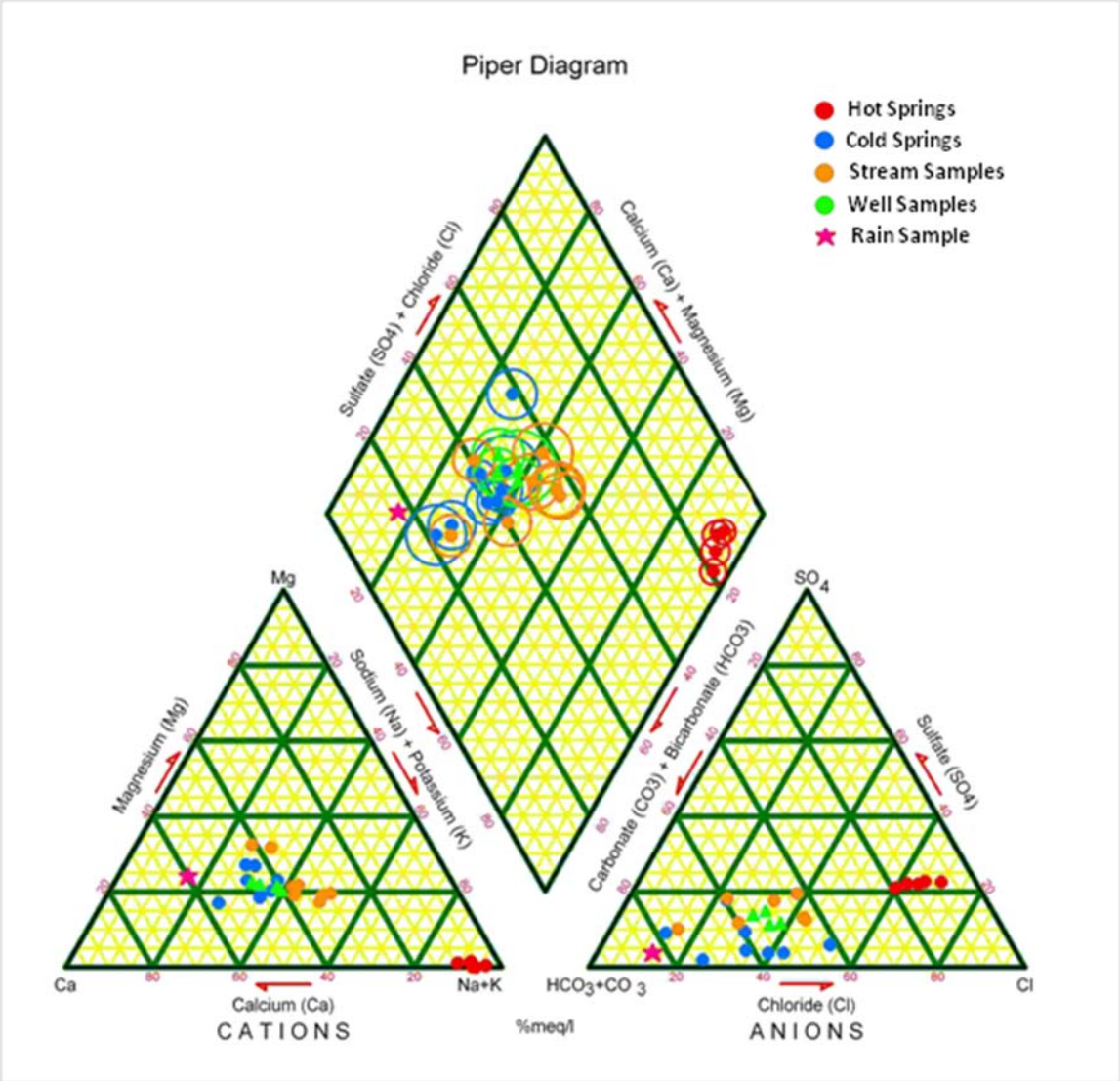

Figure 25. Piper diagram of water chemistry for the Santo Tomás eastern sub-watershed. Two clusters can be seen in the graph: 1) the thermal system and 2) all other samples. The data suggests distinct water-rock interactions between the thermal system and all cold springs, indicating two different flow systems. The stream samples near the thermal springs lose their chemical signature as they quickly mix with the surrounding elements. Note: the circle around each sample represents relative concentrations of TDS (the larger the circle, the higher the TDS).

III. 5 Environmental Isotopes ($\delta^{18}O$ and δD)

Most samples analyzed for stable isotopes ($\delta^{18}O$ and δD) plot on or near the GMWL, ranging from -8.4 to -4.2‰ for δ18O and from -53 to -19‰ for δD (Table VI) (Figure 26). Data cluster into 3 general groups: thermal waters, cold waters and the El Álamo well sample. In addition, a group of enriched (i.e., evaporated) samples are present; these consist mostly of stream samples.

"Stream samples (dry)" and "Stream samples (wet)" were collected at the same location, between 1 and 5 km downstream of the thermal springs. The "dry" samples are from October 2008 and presumably contain only thermal water, whereas the "wet" samples were taken in March 2009, and consisted of a combination of runoff from multiple storms as well as thermal water. The wet samples (denoted by yellow circles in Figure 26) plot on the GMWL and slightly higher than the dry samples (denoted by orange circles), which plot to the right of the GMWL (Figure 26).

"Stream (upstream)" samples were taken upstream from the thermal spring system in May 2009. Two of these samples (#16 and #16a), which were taken near one another along a side branch of the main arroyo, plot within the "central" cluster (denoted by purple circles in Figure 26). The other two samples (#17 and 18), which were taken near one another along the main arroyo, plot within the "evaporated" cluster (Figure 26).

Table VI. $\delta^{18}O$ and δD values in ‰ for all samples. "Stream (upstream)" refers to stream samples taken upstream from the thermal system. These were only taken during the wet season, given that they were not flowing during the dry season. The stream samples downstream of the thermal system were taken during both the "dry" and "wet" season for comparison purposes.

Sample	Type	Elevation	$\delta^{18}O$ ‰	δD ‰	Name
1	Thermal Spring	498	**-8.3**	**-53**	Agua Caliente
2	Thermal Spring	483	**-8.2**	**-52**	Warm Spring
3	Thermal Spring	495	**-8.4**	**-52**	Diffuse Warm
4	Cold Spring	636	**-6.7**	**-42**	Telnor
5	Cold Spring	426	**-6.1**	**-41**	U-Turn
6	Cold Spring	400	**-6.0**	**-38**	Ricardo
7	Cold Spring	550	**-6.6**	**-40**	Ulises
8	Cold Spring	356	**-6.4**	**-39**	Rigo
9	Cold Spring	394	**-6.1**	**-39**	Rigo Canyon
10	Cold Spring	520	**-6.9**	**-46**	Mark
11	Cold Spring	541	**-6.3**	**-43**	Don Luis
12	Well (dry)	315	**-6.7**	**-45**	Ulises (Dry)
12a	Well (wet)	315	**-6.5**	**-42**	Ulises (Wet)
13	Well	358	**-5.0**	**-34**	Rigo
14	Well	1112	**-7.3**	**-54**	El Álamo
15	Stream (dry)	410	**-6.4**	**-45**	Bronco (Dry)
15a	Stream (dry)	410	**-6.8**	**-47**	Bronco (Dry)
15b	Stream (dry)	410	**-7.0**	**-48**	Bronco (Dry)
15c	Stream (wet)	410	**-6.5**	**-42**	Bronco (Wet)
15d	Stream (wet)	410	**-6.5**	**-42**	Bronco (Wet)
16	Stream (upstream)	567	**-6.7**	**-44**	UpstreaMark
16a	stream (upstream)	567	**-7.0**	**-43**	Upstrea Mark
17	Stream (upstream)	642	**-5.7**	**-42**	El Salto
18	Stream (upstream)	610	**-4.8**	**-36**	Dwnstrm Salto
19	Pond	480	**-4.6**	**-39**	Pond 1
20	Pond	480	**-5.2**	**-41**	Pond2
21	Rain	600	**-4.2**	**-19**	Rain

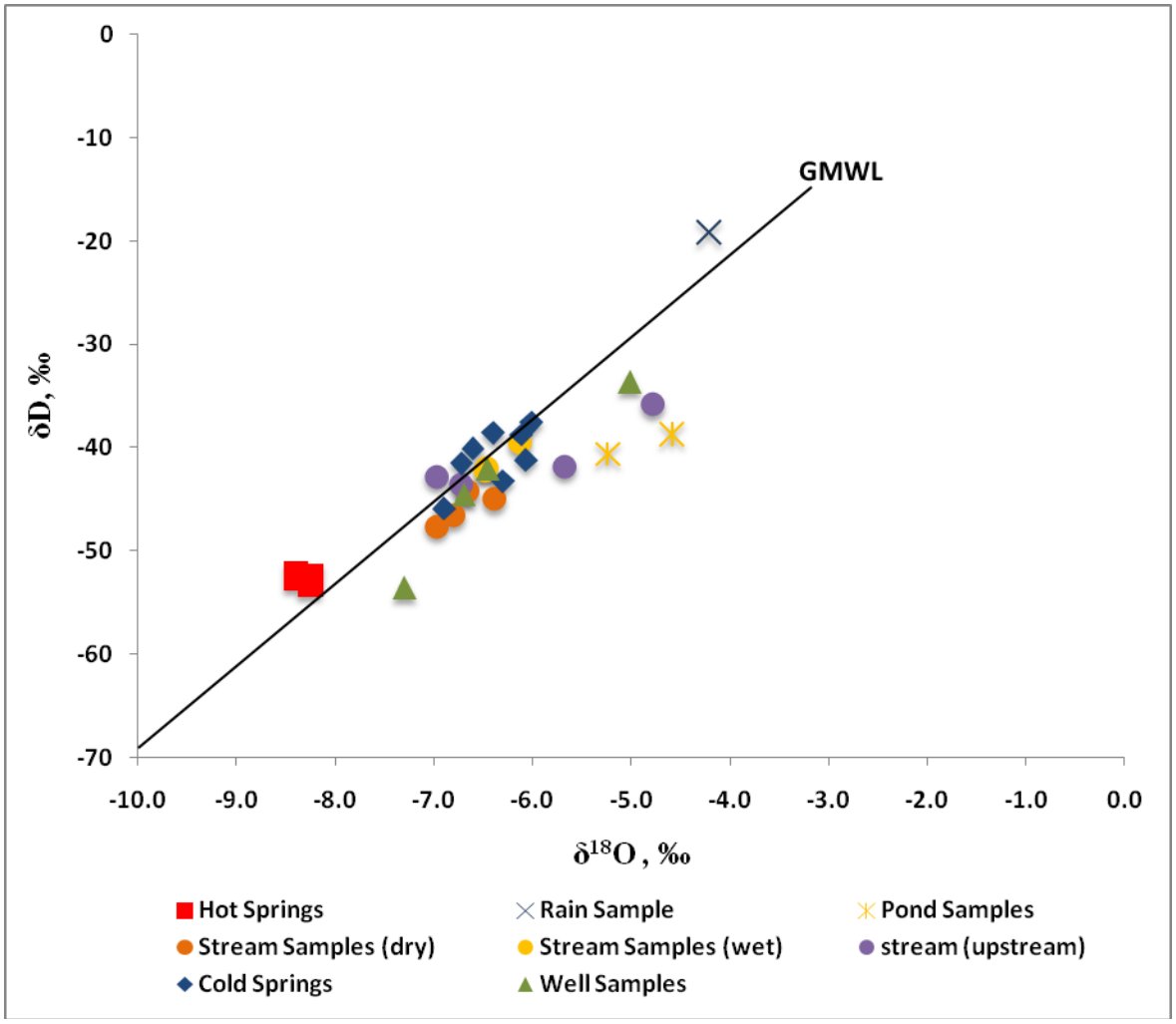

Figure 26. Plot of δD vs. $\delta^{18}O$ showing all samples taken throughout the Santo Tomás eastern sub-watershed. Samples include spring water, stream water, groundwater, and one rain sample. Samples are expressed in ‰. A "Global Meteoric Water Line" (GMWL) is shown as a reference. Stream samples (wet) and Stream Samples (dry) are samples taken at the same location, but taken at different times, specifically, during the wet and dry seasons, respectively. Stream (upstream) samples were taken upstream of the thermal spring system. The rain sample, which plots in the upper right corner, was taken during a single storm event at 520 meters elevation.

III. 6 Tritium Analysis

Tritium concentrations for the thermal spring (sample #1) and cold spring (sample #8) were below detection limits (<0.6 TU) (Table VII). These results are consistent with sub-modern recharge (prior to 1952) (Table VIII). However, modern waters for the study area may contain undetectable amounts of tritium as well (Eastoe, personal communication, 2009). Therefore, the "age" (i.e. residence time) for the springs cannot be determined using only tritium data.

Table VII. Tritium concentrations for spring samples.

Sample Number	Tritium Concentration
1 (Hot Spring)	< 0.6 TU
8 (Cold Spring)	< 0.6 TU

Table VIII. Table comparing tritium concentrations and "age" of water.

For coastal and low latitude regions (Clark and Fritz, 1997):

< 0.8 TU	Submodern - recharged prior to 1952
0.8 to ~2 TU	Mixture between submodern and recent recharge
2 to 8 TU	Modern (< 5 to 10 years)
10 to 20 TU	Residual "bomb" ^{3}H present
> 20 TU	Considerable component of recharge from 1960's or 70's

III. 7 Thermal Spring Discharge

Based on the 8 separate measurements made from November 2008 to August 2009, the thermal spring discharge ranged from 2.7 – 3.4 liters per second (Figure 27). The spring flow is fairly constant and appears to behave independently of local precipitation. However, the increased discharge in January 2009 (3.4 l/s) may be related to a heavy rainstorm (~10 cm) on December 17. If so, this result would question the nature of the spring with regard to modern precipitation.

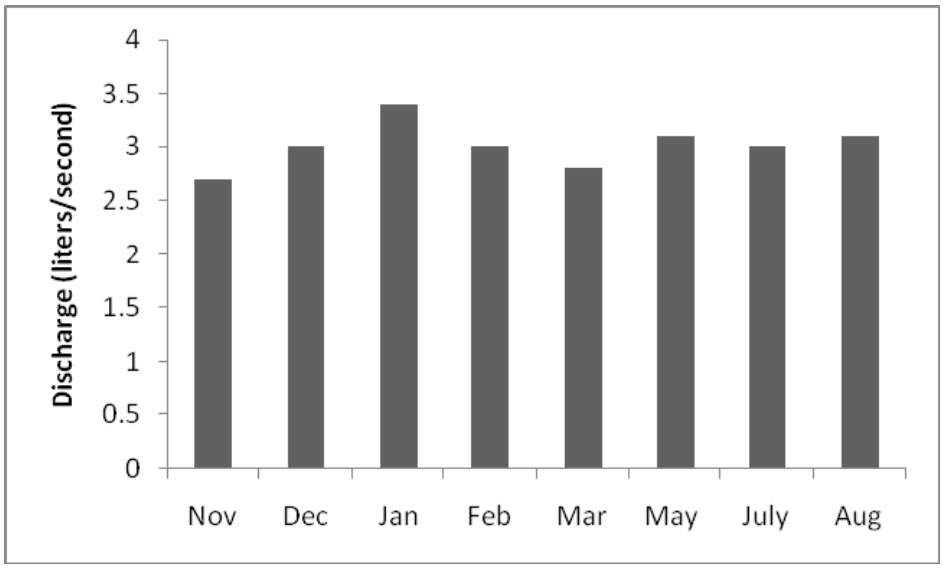

Figure 27. Discharge of the dominant thermal spring (sample 1) from the study area. At least one measurement was taken for each month shown from November 2008 to August 2009. The spring does not appear to have much of a monthly or annual discharge fluctuation. However, the increased discharge in January 2009 (3.4 l/s) may be related to a heavy rainstorm (~10 cm) on December 17, 2008

The 5 measurements from the 14-hour period on December 19, 2008 ranged from 2.9 – 3.2 liters per second (Figure 28). This fluctuation may be attributed to the spring's natural discharge or to rough measuring techniques.

Although flow from other springs was not measured, 7 of the 8 cold springs appeared to fluctuate throughout the year, displaying higher flow rates during the wet season.

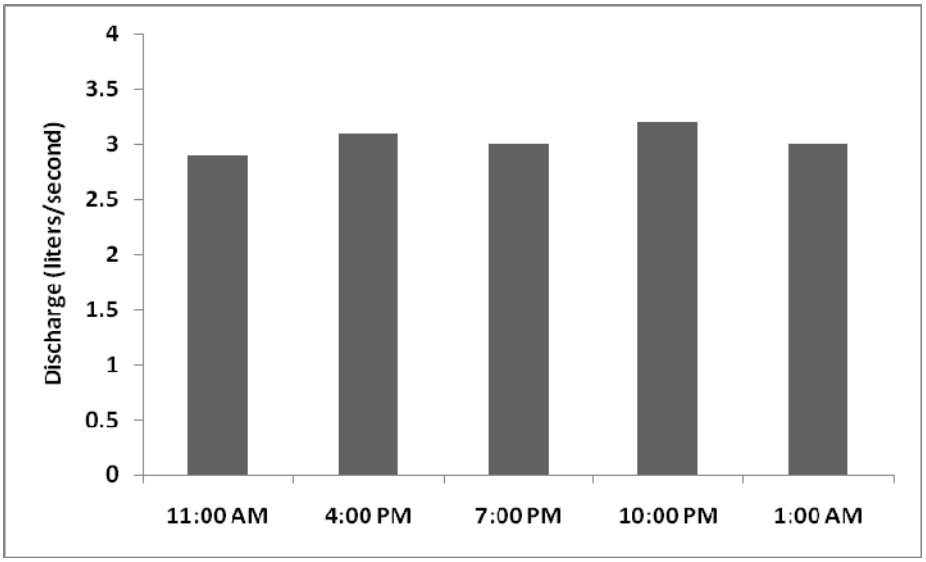

Figure 28. Discharge over a 14-hour period in December 2008. The estimates range from 2.9 – 3.2 l/s, which most likely accounts for the spring's natural discharge fluctuation or measuring error.

IV. DISCUSSION

Based on stable isotope data, the Santo Tomás eastern sub watershed has three distinct types of water. The first type is primarily represented by the thermal springs in the lower portion of the sub-watershed, but also includes ambient temperature waters of similar origin. The second type is characterized by the cold springs, also low in the sub-watershed. Finally a third type is characterized by a well water sample at higher elevation and near the eastern boundary of the watershed in the town of El Álamo. Each of these water-types recharges the valley aquifer as MBR. The differences between the waters might be due to distinct types and areas of recharge in the mountain system. Discussing the spatial, physical and chemical characteristics for each of the water types will provide insight into the hydrologic processes (e.g., type of recharge, source of recharge etc.) within the mountain-block-dominated watershed.

IV.1 Focused and Diffuse MBR in the Study Area

Cold Springs

All 8 cold springs are located near significant fractures within the mountain block. These fractures are likely groundwater conduits for cold spring-type water for the area. Stable isotope data show 5 of these springs plot near the GMWL, with no sign of isotopic enrichment (i.e., evaporation) (Figure 29). Rapid infiltration into the nearby fractures will produce the observed isotopic data. These 5 springs should be considered *focused* MBR.

The other 3 springs have undergone a slight degree of enrichment (Figure 29). These springs are also recharged within the mountain block; however, their infiltration process may be influenced by a combination of the lithology and fractures within the mountain system. Therefore, these springs are likely recharged by a *diffuse* and *focused* mountain-*block* component.

Thermal Spring-Type Water

Stable isotope data of the thermal springs plot near the GMWL, and show no sign of enrichment (Figure 29). This result indicates the water is little affected by local aridity and likely infiltrates into the sub-surface rapidly. A source of recharge for the springs may be in highly permeable faulted and/or fractured rock. The active fault located within meters of the thermal springs (Figure 22) most likely act as a conduit for the waters at depth. Based on these results, the thermal springs should be considered *focused* MBR. Groundwater in areas with low or 0 slope will most likely undergo evaporation during infiltration, and would not contribute water to the thermal springs.

El Álamo

Stable isotope data show the El Álamo sample has undergone enrichment (Figure 29), which can be attributed to slow infiltration. Increased concentrations of Ca, Mg, K, and TDS for the sample may indicate extended periods of water-soil interaction (Table V). Based on these results, the El Álamo sample likely is recharged in a diffuse manner.

Fractured/weathered granitic rock is abundant in and around the El Álamo area (Figure 20). Groundwater flow may not concentrate along faults in this area. Instead, groundwater may infiltrate through the granite in a diffuse manner (i.e., diffuse MBR). Moreover, in low slope areas, this fractured rock is overlain by a thick sediment cover, which will decrease infiltration rates. Combined, these physical features favor diffuse MBR.

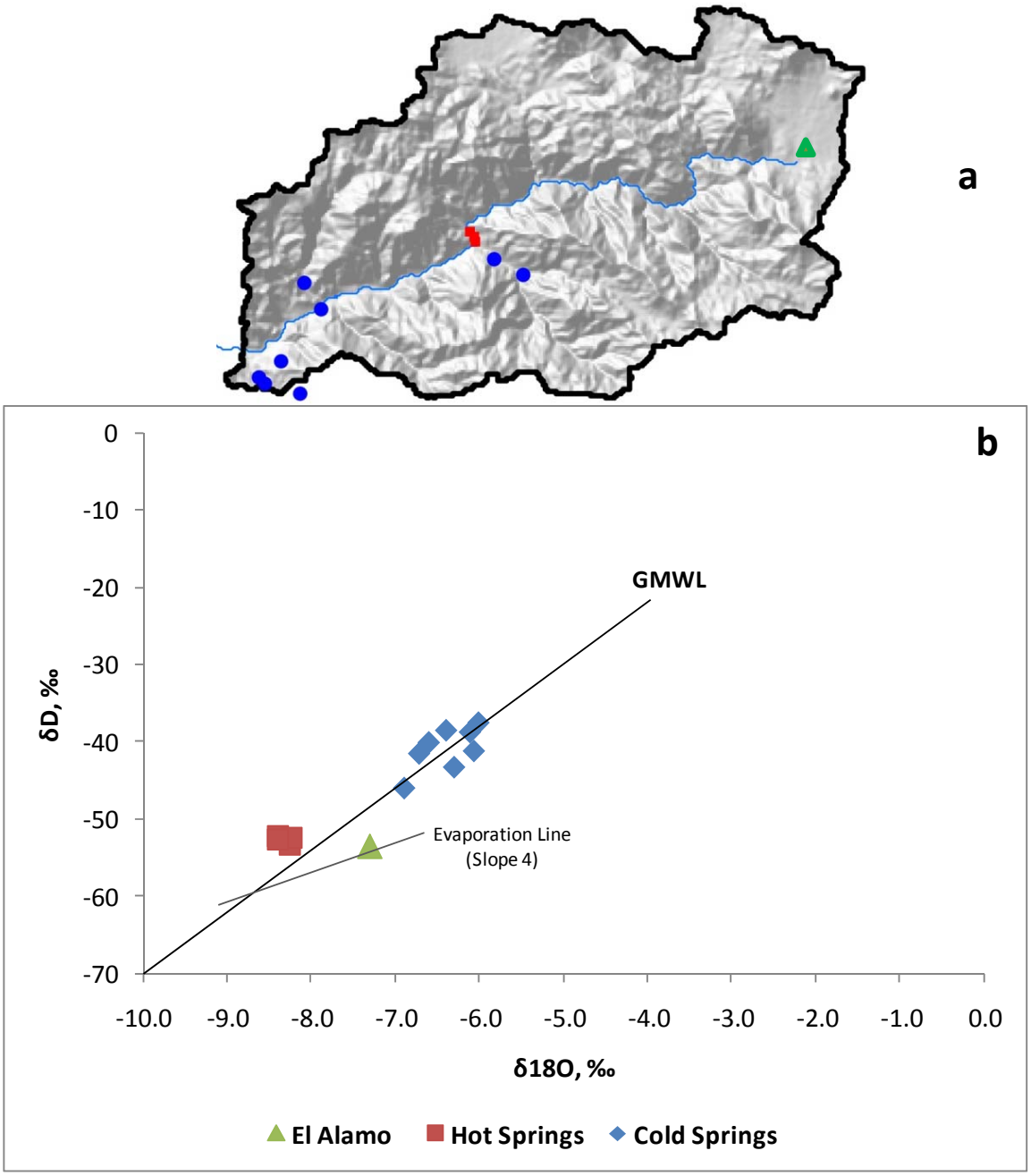

Figure 29. a) Map of the study area with the locations of cold springs, thermal springs and El Álamo samples. b) 3 types of water shown that exist with the study area. The first type is represented by the thermal springs. The second type is characterized by the cold springs. Finally a third type is characterized by a well water sample at higher elevation and near the eastern boundary of the watershed in the town of El Álamo.

IV. 2 Sources of MBR and Origin of the Waters in the Study Area

Cold Springs

The 8 sampled cold springs contain low concentrations of major cations/anions and TDS, indicating the spring water undergoes minimal water-rock interaction (Table V). These low concentrations may be related to proximal (i.e., local) groundwater flow paths within in the mountain block. Discharge from 7 of the 8 springs fluctuates throughout the year; these appear to be influenced by local, modern precipitation. Based on these data and observations, the source of recharge for each of the 7 springs originates from *local flow paths* within the mountain block.

If each spring is recharged from local flow, and therefore local precipitation, then there may be a relationship between the elevation of each spring and the corresponding $\delta^{18}O$ value (Table IX). This relationship was used to derive an altitude effect for the area (Figure 30). (Data on the isotopic composition of local precipitation are typically used to derive altitude effects, but were not available for the area).

Two altitude effects were derived: 1) 0.22‰ $\delta^{18}O$ depletion (per 100-m rise in elevation) based on data from all 8 cold springs, and 2) 0.30‰ $\delta^{18}O$ depletion, omitting sample #8. This sample is the only non-diffuse cold spring, and may not represent local groundwater flow. The two derived values represent the possible range of the likely altitude effect for the area.

Table IX. Elevation of cold springs at their respective discharge point and corresponding $\delta^{18}O$ value.

Sample	Type	Elevation	$\delta^{18}O$	Name
8	Cold	356	-6.4	Rigo
9	Cold	394	-6.1	Rigo Canyon
6	Cold	400	-6.0	Ricardo
5	Cold	426	-6.1	U-Turn
10	Cold	520	-6.9	Mark
11	Cold	541	-6.3	Don Luis
7	Cold	550	-6.6	Ulises
4	Cold	636	-6.7	Telnor

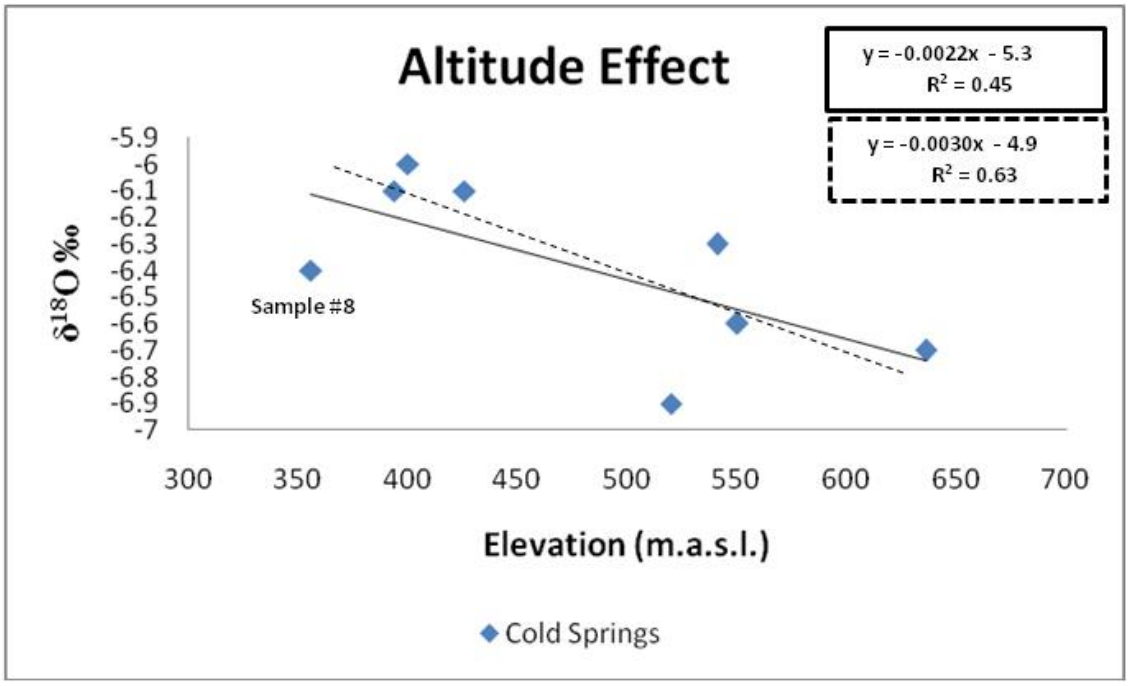

Figure 30. The relationship between each of the 8 cold springs elevation (at its discharge point) and its corresponding $\delta^{18}O$ value. Two regression lines were calculated: one including all 8 cold springs (solid line), and one (dashed line) omitting sample #8, which is the only non-diffuse cold spring, and may not represent local groundwater flow. The results represent a range of a possible "altitude effect" for the area. Results range from -0.22‰ $\delta^{18}O$ depletion per 100-m rise in elevation based on all 8 spring samples and a -0.30‰ $\delta^{18}O$ depletion rate after omitting sample #8. The two derived values represent the possible range of the likely altitude effect for the area.

Thermal Springs

Stable isotope data suggest the source of recharge for the thermal springs differs from that of the cold springs. The thermal springs are near the cold springs spatially, yet an average $\delta^{18}O$ difference of 1.9‰ exists between the two groups (Figure 29). The thermal springs have undergone a significant depletion in heavy isotopes. This depletion can be explained in various ways: 1) the thermal springs might contain paleo-groundwaters; 2) the thermal springs might be recharged at higher elevations than the cold springs (i.e. altitude effect) or 3) some combination of 1 and 2 may exist.

Eastoe et al., [2008] show that the most depleted isotope samples in the Hueco Bolson aquifer (Mexico/Texas international border) are most likely from late Pleistocene precipitation (Darling et al., 1998). A similar situation is seen with the thermal waters in the Santo Tomás eastern sub-watershed. However, the thermal springs contain low concentrations of major cation/anion and TDS (Table V). These results contradict the assumption of paleo-groundwaters. Therefore, an altitude effect is a likely explanation for the isotope data.

To help determine the source of recharge for the thermal springs, the derived altitude effects were applied to the isotope data. Results show that the thermal springs are being recharged from a source ~600 to 900 m higher than the average source of the cold springs, or elevations of ~1100 to 1400+ meters above sea level (m.a.s.l.).

The Santo Tomás watershed has an average elevation of 1040 m.a.s.l, and a maximum elevation of ~1660 m.a.s.l (Table III). The areas represented by the highest altitudes are limited in the study area, and most likely unable to transmit significant amounts of water. Therefore, the thermal system is likely being recharged from a higher source located outside of the Santo Tomás watershed boundary. The altitudes needed to produce the $\delta^{18}O$ result would likely come from the Sierra Juárez Mountain Range, where elevations reach ~1800 m.a.s.l. Based on the type of recharge for the thermal springs (*focused* mountain-*block*), faults and fractures may provide a sub-surface medium capable of transporting

groundwater over long distances (e.g., ~40 km from the Sierra Juárez Mountains to the thermal spring point of discharge).

Assuming the thermal springs are being recharged from long distances (~40 km), water may reside in the mountain block for decades. Residence times of 70+ years is consistent with the low tritium concentrations (<0.6 TU) seen in the thermal spring (Table VII). The elevated temperatures (49^0C), increased Sodium content (Figure 24) and steady discharge of the thermal spring (Figure 27) all supports a deep, extensive groundwater flow regime. Based on the chemical, geological, topographic and hydrologic data, thermal spring-type water likely travels through a complex fault/fracture system, at depth, and should be considered *regional* mountain block *flow*.

El Álamo

The El Álamo sample was collected at 1114 m.a.s.l., and was depleted in heavy isotopes (Figure 29). This depletion is consistent with high altitudes, which are common along the eastern section of the watershed. The isotope data is likely related to the elevation of recharge for the El Álamo sample, and can be used to help determine the source of recharge for El Álamo-type water.

To calculate the recharge elevation for the El Álamo sample, the original isotopic composition (before evaporation) must be known. The isotopic enrichment caused by evaporation has displaced the sample from the GMWL. An evaporation line (of slope 4) was assumed for the area, and used to "regress" the sample back to the GMWL and determine the water's isotopic origin (Figure 29).

Results show a δ^{18}O value of approximately -8.8‰ for the El Álamo sample. When applied to the derived altitude effects, the δ18O value implies that the El Álamo groundwater is being recharged from a source located at ~1300 to 1600+ m.a.s.l. These results suggest the El Álamo sample may be recharged from areas higher in elevation than can be found in the Santo Tomás watershed. The water likely comes from altitudes located beyond the

topographic watershed boundary. These results imply that the watershed boundary and the groundwater recharge boundary to not coincide for this area.

IV. 3 Focused MFR in the Study Area

Overview

The hydrologic processes within the mountain block were discussed in the preceding section in terms of 3 water types. These waters most likely recharge the Santo Tomás Valley aquifer as *sub-surface* lateral inflow (i.e. MBR).

The following discussion will concentrate on *near-surface* recharge (i.e. MFR) in the lower portion of the study area. A likely component of MFR might originate as overland flow along the Santo Tomás arroyo. A portion of flowing water infiltrates the alluvial stream bed and becomes groundwater. This type of recharge is considered a *focused* mountain-*front* component. To determine the processes controlling this type of recharge in the study area, stream water, aquifer and pond samples were analyzed.

Overland flow in the arroyo may originate from surface runoff after storm events. This flow may recharge the valley aquifer during wet years, but is absent during dry years. On the other hand, spring discharge near the arroyo flows year-round, and might contribute water to the valley aquifer during dry years. In particular, the steady discharge from the thermal springs might be an important source of groundwater for the local valley aquifer during these dry years.

After surfacing, the springs flow downstream and form a perennial stream (as seen in figure 31a) for ~5 km along the Santo Tomás arroyo before 1) infiltrating into the alluvial aquifer, 2) evaporating or 3) being used by plants (transpiration). Once the thermal springs surface, they become susceptible to evapotransipiration, lowering their contribution to local groundwater. A study in southern California's Mojave Desert estimates that only one-tenth of actual stream flow over a ~15 km stretch becomes recharge; the other 90% is lost to ET

(Izbicki, 2002). The Southern California data raise questions about the significance to groundwater of *focused* mountain-*front* recharge along the Santo Tomás arroyo.

Stable isotope data comparing thermal spring-type water, perennial stream, valley aquifer and pond samples will help determine the importance of the focused MFR in study area. If the thermal waters can be traced from their origin (the spring) to the perennial stream, and ultimately to the groundwater, it would provide evidence suggesting the thermal waters successfully recharge the valley aquifer. Because the samples were taken during a dry period (October 2008), the results would reflect recharge occurring in arid conditions.

Stream Samples

Stable isotope results for the perennial stream plot to the right of the GMWL (Figure 31). This enrichment implies the water has undergone some degree of evaporation, which would be expected based on the physical conditions (i.e. channel infiltration, aridity) for stream flow.

Isotope data also show the stream samples plot below the cold springs. This result implies that cold spring-type water is not a source for the perennial stream. The thermal springs are the sole source of overland flow for the stream. Applying this knowledge, the evaporated stream samples can be traced back to their meteoric origin (i.e. thermal springs). The slope of the regression line connecting these two groups provides an evaporation slope (of 4) for the area (Figure 31). Because the samples were collected in October, this slope corresponds to an evaporation effect during arid months.

Valley Aquifer Sample

Stable isotope data show that the thermal springs supply water to the perennial stream, but does this stream water infiltrate and replenish the valley aquifer during arid months, or is the water lost through ET?

Stable isotope data from the alluvial aquifer (sample #12) plot near the stream samples (Figure 31), indicating that a portion of the perennial stream recharges the valley aquifer.

The well sample does not display a greater degree of isotopic enrichment when compared to the stream samples. This result indicates that there is little, if any, evaporation occurring within the vadose zone along the ~10 km stretch between the termination of the perennial stream and the well. However, the well sample plots slightly above the stream samples. This result might represent a mixing effect between the perennial stream and cold spring-type water. This mixing would nullify an existing isotopic enrichment within the well sample.

Despite the possible mixing of thermal spring and cold spring-type water within the well sample, stable isotope data show that the perennial stream, and therefore the thermal springs, recharge the valley aquifer as focused MFR during dry months. The significance of these thermal waters as a groundwater source largely depends on their degree of mixing with cold spring-type water.

Stream recharge is also affected by transpiration. However, transpiration is not a highly fractionating process (Zimmerman et al., 1967; Clark and Fritz, 1997) and can be difficult to trace using $\delta^{18}O$ and δD.

The well and stream were also sampled in March 2009, after the Santo Tomás arroyo had 3 months of continuous runoff from rainfall. Both samples plot higher along on GMWL, indicating a greater contribution of cold spring-type water.

Because these ponds are located ~150 m upstream from the dominant thermal spring, it implies that the thermal spring-type water is most likely contributing groundwater at depth as well as through springs. Therefore, the thermal spring-type water may be more significant than just the surfacing springs; it may be a complex system at depth, contributing significant amounts of water to the valley aquifer.

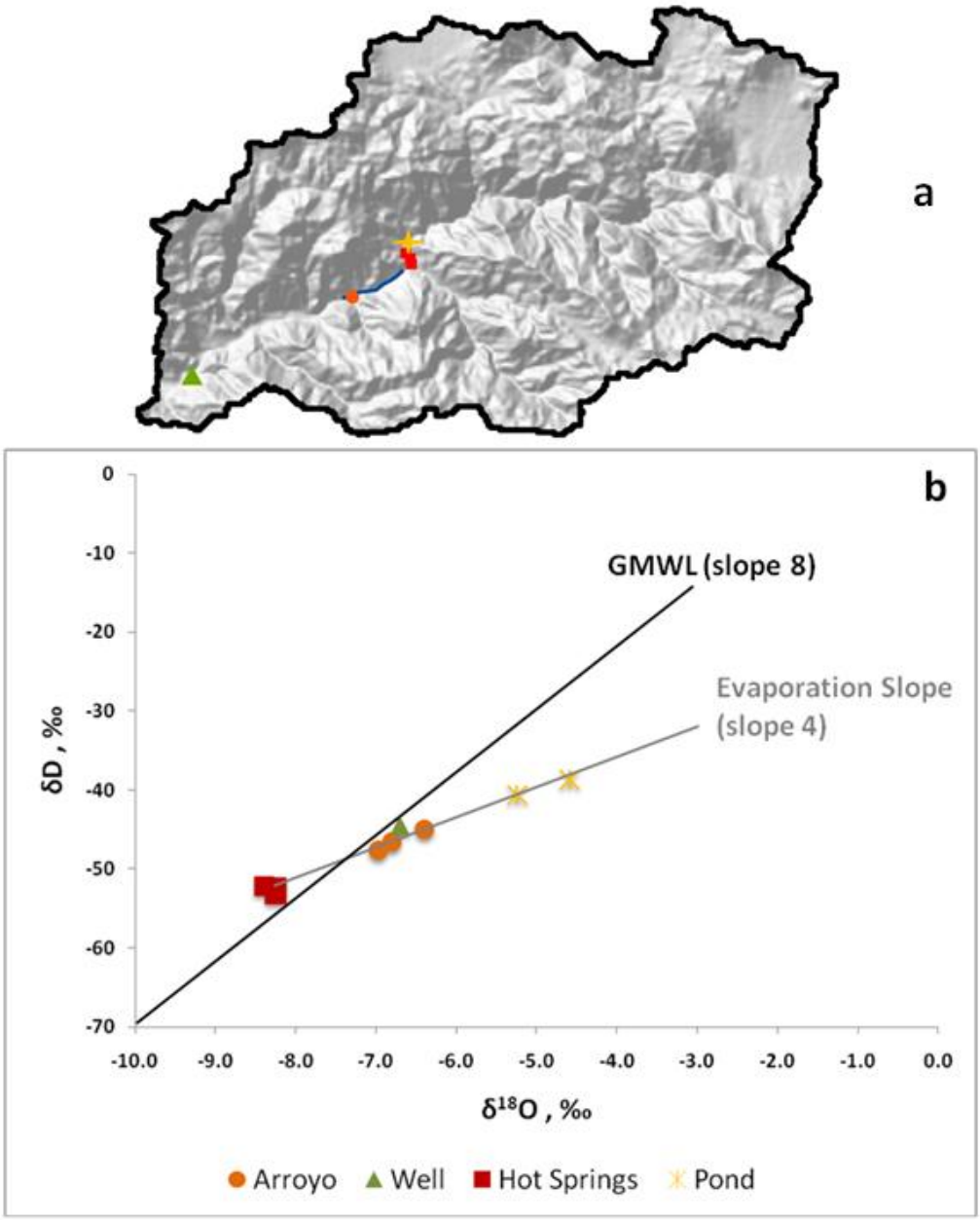

Figure 31. a) Relative locations of the hot springs, both pond samples, stream samples (during dry months) (#15) and a downstream well sample (#12). The blue line indicates the perennial overland flow from the thermal springs. b) Plot of δD vs. $\delta^{18}O$ showing the samples from the location map (a). The stream samples display an "evaporation effect". Because the stream originates at the thermal system, most of the water in the stream is thermal water; therefore, an "evaporation line" for the area can be calculated. Using this line, the pond samples can also trace back to the thermal springs (before evaporation), indicating they are from the same origin as the thermal system. Additionally, the downstream well samples plots with the stream samples, indicating the arroyo successfully recharges the valley aquifer.

Pond Samples

Isotope data for both pond samples (#19, #20), also taken in October 2008, show greater isotopic enrichment (i.e. evaporation) compared to the stream samples (Figure 31). Applying the evaporation slope for the area shows that the ponds display the same original isotopic composition as the thermal springs, indicating that both originate from the same source. The diffuse and stagnant nature of the ponds can explain their cool (ambient) temperature, as well as their increased isotopic enrichment.

IV. 4 Tracing Groundwater Using an Evaporation Slope

Stable isotope data were analyzed to try and trace water throughout the study area. A linear relationship, with slope 4, is seen between a cold spring (#9) and nearby well (#13) (Figure 32). This result indicates the well is dominantly recharged from cold-spring type water (in particular spring #9). The enriched well sample was collected on an ancient river terrace ~5 m higher than the Santo Tomás arroyo. The well is near located downstream of the thermal system, yet it does not appear to contain thermal spring-type water. This relationship helps verify an evaporation slope of (4) for the area, and provides information as to the extent of MFR of thermal spring-type water.

Two low-flowing stream samples (#17, #18), taken upstream of the thermal system in May 2008, appear to be perennial flowing systems (possibly diffuse spring systems). Stable isotope data suggest that both samples have undergone evaporation (Figure 32). Appling an evaporation slope 4 to the samples implies they are being recharged by cold spring-type water. However, the samples were collected in May, and a steeper evaporation slope might be appropriate for the samples. A steeper evaporation line (shown as a dotted line in Figure) would imply a connection with El Álamo or thermal spring-type water. The stream samples are located, spatially, between the higher eastern section of the study area and lower western section. They may provide information connecting El Álamo-type water with cold spring and/or thermal spring-type water. If so, they will help to understand mountain block flow throughout the study area.

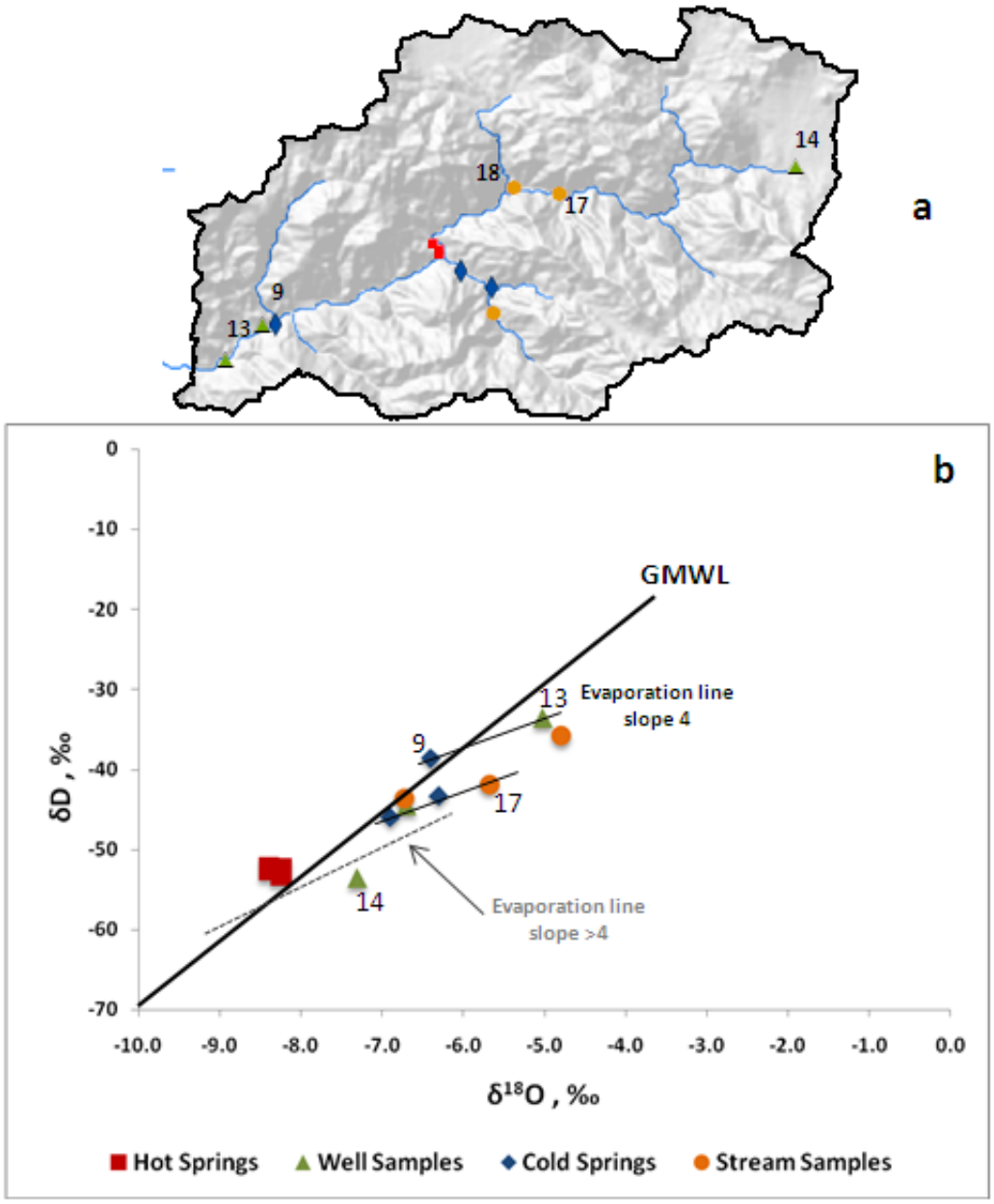

Figure 32. a) Location map showing samples from graph below. b) Map showing 2 evaporation lines (slope 4). The upper line shows a direct relationship between spring 9 and well 13. The well appears to be recharged from the nearby spring, and not by the thermal system (unlike the nearby well, found further downstream). Samples 17 and 18 also show a direct relationship with cold spring-type water based on the lower evaporation line of slope 4. However, if the evaporation slope is steeper (shown by the dotted line) for these samples, they may originate from El Álamo-type water.

IV. 5 Using Basin Characterization to Understand MBR

Geologic components that make up the Santo Tomás watershed help understand the physical processes controlling MBR. Active faults in the study area transmit a part of the water within the mountain block. The thermal spring-type water likely moves along active faults and/or fractured crystalline rock. The heavily fractured rock in the study area can provide a medium for water circulation at a depth of at least 4-5 km (Gastil and Bertine, 1986). These depths easily explain the elevated temperatures of the water. Regions of the watershed with increased fault/fracture density may therefore help determine areas of increased MBR.

A map showing NDVI during a "dry" period (e.g., October) can be a useful tool in identifying spring water and/or active faults for the area. The method relies on indentifying areas with a sharp contrast between bare rock and live green vegetation. This contrast is indicative of spring water. Applying this criterion, a NDVI may help determine areas where MBR is prevalent within the mountain system.

V. CONCLUSIONS

MBR is an important source of groundwater for the mountain-block dominated Santo Tomás eastern sub-watershed. Stable isotope data from this study display various isotopic effects which provide insight into the hydrologic processes within the mountain system. Additionally, basin characterization data and major cation/anion data supplement the study to help understand MBR and MFR in the study area. Results from this study include:

1. Three distinct types of water exist within the study area: 1) cold spring-type water, which represents local flow within the mountain block and is considered focused and/or diffuse MBR; 2) thermal spring-type water, which represents regional flow within the mountain block. This water-type is associated with active faults, and is considered focused MBR, and 3) El Álamo-type water, which represents groundwater along the eastern boundary of the watershed. These depleted isotopic waters are considered diffuse MBR. They do not appear to be fault related; instead, local lithology and topography influence recharge in this area.

2. The Santo Tomás Valley aquifer is being recharged via the mountain block (i.e. MBR) from water whose source originates outside the watershed boundary. Based on a derived "altitude effect", which is between -0.30 and -0.22 $\delta^{18}O‰$ depletion (per 100-m rise in elevation), the thermal spring-type water is being recharged from a source located ~1100-1400+ m.a.s.l. These altitudes are mostly found ~40 km east of the watershed boundary in the Sierra Juárez Mountain Range. The El Álamo-type water is also likely being recharged from a source located east of the watershed boundary at ~1300-1600+ m.a.s.l. This result implies that the watershed boundary and the groundwater recharge boundary do not coincide for this area, and the Santo Tomás Valley aquifer may receive a substantial amount of water from MBR.

3. The surfacing thermal spring's discharge is relatively steady year-round, and successfully recharges the local valley aquifer as MFR during "dry" years. Tracing the

thermal spring water throughout the course of a 5 km-long perennial stream enabled me to assign an evaporation line (of slope 4) for the area. (This slope applies to the area for the month of October). Applying this slope, I was able to determine that the stagnant pond samples (found upstream of the thermal springs) are from the same distant origin as the thermal springs. This result implies that the thermal spring-type water may be more significant than surfacing thermal springs; it may be a complex system at depth, contributing significant amounts of water the valley aquifer.

4. There is a direct relationship between active faults and springs within the watershed. A map displaying only active faults may be a useful tool in hydrologic studies for the Santo Tomás Valley region.

5. A map showing NDVI during a "dry" period (e.g., October) can be a useful tool in identifying spring water and/or active faults for the area. This method relies on indentifying areas with a sharp contrast between bare rock and live green vegetation. This contrast is indicative of spring water.

Suggestions for Further Study

Knowledge of the hydrologic process within a mountain block can provide detailed information as to the source and significance of groundwater in mountain-block dominated catchments. To better understand this process in the Santo Tomás valley and in northern Baja California, an accurate "altitude effect" should be derived for the region. Isotope data from multiple rain samples from various elevations throughout the watershed and throughout northern Baja California can significantly help understand MBR for this mountainous region. Furthermore, tritium analyses (with a >0.2 TU detection limit) and/or CFC analyses of the spring and well water can provide the residence time for spring and groundwater samples. This information will help understand the flow rates within the mountain block. Combined with geologic information and stable isotope data, these rates can help provide permeability values within the mountain system; this knowledge will help promote groundwater management and sustainability for the region.

REFERENCES

Allen, C.R., Silver, L.T., and Stehli, F.G., 1960. Agua Blanca fault – A major transverse structure of northern Baja California, Mexico: Geological Society of America Bulletin, 71(4): 457-482.

Caine, J.S., Evans, J.P., and Forster, C.B., 1996. Fault zone architecture and permeability structure. Geology, 24(11): 1025-1028.

Charles-Edwards, D., and O'Keeffe, S., 2003. An Australian Environmental Handbook. Sci-plan pty ltd.

Clark, I. and Fritz, P. 1997. Environmental Isotopes in Hydrogeology. Lewis Publishers, New York.

Comisión Nacional del Agua, 2008. Determinación de la disponibilidad de agua subterránean en el acuífero Santo Tomás, estado de Baja California. In: Organismo de Cuenca Peninsula de Baja California

Craig, H., 1961b. Isotopic variations in meteoric waters. Science, 133: 1702-1703

Dansgaard, W., 1964. Stable isotopes in precipitation. Tellus, 16: 436-468.

Darling, B.K., Hibbs, B.J., and Sharp, J.M., 1998. Environmental isotopes as indicators of residence time of ground waters in the Eagle Flat and Red Light Draw basins of Trans-Pecos Texas. In: DeMis, W.D., Nelis M.K. (eds) The search continues into the 21st century. West Texas Geological Society Fall Symposium, West Texas Geol Soc Publ 98-105: 259-270.

Eastoe, C.J., Gu, A., and Long, A., 2004. The origins, ages and flow paths of groundwater in Tucson Basin: results of a study of multiple isotope systems. In: Hogan J.F., Phillips, F.M., and Scanlon, B.R., (eds) Groundwater Recharge in a Desert Environment: The Southwestern United States. American Geophysical Union Water Science and Application 9: 217-234.

Eastoe, C.J., Hibbs, B.J., Olivas, A.G., Hogan, J.F., Hawley, J., and Hutchison, W.R., 2008. Isotopes in the Hueco Bolson aquifer, Texas (USA) and Chihuahua (Mexico): local and general implications for recharge sources in alluvial basins. Hydrogeology Journal, 16: 737-747.

Flint, A.L., Flint, L.E., Hevesi, J.A., and Blainey, J.B., 2004. Fundamental concepts of recharge in the Desert Southwest: a regional modeling perspective. In: Hogan J.F., Phillips, F.M., and Scanlon, B.R., (eds) Groundwater Recharge in a Desert Environment: The Southwestern United States. American geophysical Union Water Science and Application 9: 159-184.

Gastil, R.G., Phillips, R.P., and Allison, E.C., 1975. Reconnaissance geology of the state of Baja California, Mexico: Geological Society of America Memoir 140, 170 pp.

Gastil, R.G., and Bertine, K., 1986. Correlation between seismicity and the distribution of thermal and carbonate water in southern and Baja California, United States and Mexico. Geology, 14: 287-290.

Huntley, D., 1979. Groundwater recharge to the aquifers of northern San Luis Valley, Colorado. Geological Society of America Bulletin, Part II, 90(8): 1196-1281.

Izbicki, J.A., 2002. Geologic and hydrologic controls on the movement of water through a thick, heterogeneous unsaturated zone underlying an intermittent stream in the western Mojave Desert, southern California, Water Resources Research, 38: 21-214.

Keith, S.J., 1980. Mountain front recharge: in Wilson, L.G., et al., (eds) Regional Recharge Research for Southwest Alluvial Basins, pp.4-1 to 4-44, Chapter 4, Tucson, University of Arizona.

Manning, A.H., and Soloman, D.K., 2004. Constraining mountain-block recharge to the eastern Salt Lake Valley, Utah with dissolved noble gas and tritium data. In: Hogan J.F., Phillips, F.M., and Scanlon, B.R., (eds) Groundwater Recharge in a Desert Environment: The Southwestern United States. American geophysical Union Water Science and Application, 9: 139-158.

Maurer, D.K., Prudic, D.E., Berger, D.L., and Thodal, C.E., 1999. Sources of water flowing into basin-fill aquifers underlying Carson City, Nevada, Geological Society of America, Annual Meeting, Abstracts with Programs, 31(7): 87.

Michel, R.L., 2005. Tritium in the hydrologic cycle. In: Aggarwal, P.K., Gat, J.R., and Froehlich, K.F.O., (eds) Isotopes in the Water Cycle: Past, Present and Future of a Development Science, 53-66.

Morawitz, D.F., Blewett, T.M., Cohen, A., and Alberi, M., 2006. Using NDVI to assess vegetative land cover change in Central Puget Sound. Environmental Monitoring and Assessment, 114: 85-106.

Palmer, P.C., Gannett, M.W., and Hinkle, S.R., 2007. Isotopic characterization of three groundwater sources and inferences for selected aquifers in the upper Klamath Basin of Oregon and California, USA. Journal of Hydrology, 336: 17-29.

Phillips, F.M., Hogan, J.F., and Scanlon, B.R., 2004. Introduction in overview. In: Hogan J.F., Phillips, F.M., and Scanlon, B.R., (eds) Groundwater Recharge in a Desert Environment: The Southwestern United States. American geophysical Union Water Science and Application, 9: 1-14.

Ponce, V.M., Pandey, R.P., and Kumar, S., 1999. Groundwater recharge by channel infiltration in El Barbon basin, Baja California, Mexico. Journal of Hydrology, 214: 1-7.

Rockwell, T.K., Schug, D.L., and Hatch, M.E., 1993. Late Quaternary slip rates along the Agua Blanca fault, Baja California, Mexico. In: (P.L. Abbott, ed) Geological Investigations of Baja California: South Coast Geological Society, Annual Field Trip Guidbook No.21: 53-92.

Scanlon, B.R., Keese, K.E., Flint, A.L., Flint, L.E., Gaye, C.B., Edmunds, W.M., and Simmers, I., 2006. Global synthesis of groundwater recharge in semiarid and arid regions. Hydrological Processes, 20: 3335-3370.

Siegel, D.I., 1991. Evidence for dilution of deep, confined ground water by vertical recharge of isotopically heavy Pleistocene water. Geology, 19: 433-436.

Smerdon, B.D., Allen, D.M., Grasby, S.E., and Berg, M.E., 2008. An approach for predicting groundwater recharge in mountainous watersheds. Journal of Hydrology, 365: 156-172.

Smith, S.V., Bullock, S.H., Hinojosa-Corona, A., Franco-Vizcaino, E., Escoto-Rodriguez, M., Kretzschmar, T.G., Farfán, L.M., and Salazar-Ceseña, J.M., 2006. Soil erosion and significance for carbon fluxes in a mountainous Mediterranean-climate watershed. Ecological Applications, 17(5): 1379-1387.

Suárez-Vidal, F. 1993. Marco estructural de la falla Agua Blanca, Baja California, Mexico. In: Delgado-Argote, L.A., and Martin-Barajas, A. (eds.), Contribuciones a la Tectonica de Occidente de Mexico: Monografia No.1 Union Geofisica Mexicana, 1993, p.24-39.

Sukhija, B.S., Reddy, D.V., Nagabhushanam, P., Bhattacharya, S.K., Jani, R.A., and Kumar, D., 2006. Characterization of recharge processes and groundwater flow mechanisms in weathered-fractured granites of Hyderabad (India) using isotopes. Hydrogeology Journal, 14: 663-674

Szapiro, S. and Steckel, F., 1967. Physical properties of heavy oxygen water. 2. Vapour pressure. Transactions Faraday Society, 63: 883.

Thyne, G.D., Gillespie, J.M., and Ostdick, J.R., 1999. Evidence for interbasin flow through bedrock in the southeastern Sierra Nevada. Geological Society of America Bulletin; 111: 1600-1616.

Urey, H.C., 1947. The thermodynamic properties of isotopic substances. Journal of Chemical Society: 562-581.

Wilson, J.L., and Guan, H. 2004. Mountain-block hydrology and mountain-front recharge. In: Hogan J.F., Phillips, F.M., and Scanlon, B.R., (eds) Groundwater Recharge in a Desert Environment: The Southwestern United States. American geophysical Union Water Science and Application, 9: 139-158.

Wright, W.E., 2001. δD and $\delta^{18}O$ in mixed conifer systems in the U.S. Southwest: The potential of $\delta^{18}O$ in Pinus ponderosa tree rings as a natural environmental recorder. Unpubl. Ph.D.Diss., Univ. of Arizona, Tucson, 328 pp.

Zimmerman, U., Münnich, K.O., and Roether, W., 1967. Downward movement of soil moisture traced by means of hydrogen isotopes. In: Isotope Techniques in the Hydrologic Cycle, Geophysical Monograph Series 11, American Geophysical Union.